IOP Publishing Inverse Problems

Inverse Problems **30** (2014) 075002 (27pp) doi:10.1088/0266-5611/30/7/075002

Single-polarization SAR imaging in the presence of Faraday rotation

Mikhail Gilman[1], **Erick Smith**[1,3] **and Semyon Tsynkov**[1,2]

[1] Department of Mathematics, North Carolina State University, Campus Box 8205, Raleigh, NC 27695, USA
[2] Moscow Institute of Physics and Technology, Dolgoprudny, 141700, Russia
[3] Radar Division, US Naval Research Laboratory (NRL), 4555 Overlook Ave SW, Washington, DC 20375, USA

E-mail: tsynkov@math.ncsu.edu

Received 26 July 2013
Accepted for publication 9 April 2014
Published 24 June 2014

Abstract

We discuss the single-polarization SAR imaging with the Faraday rotation (FR) taken into account. The FR leads to a reduction in the intensity of the received radar signal that varies over the signal length. That, in turn, results in a degradation of the image. In particular, the image of a point target may have its intensity peak split in the range direction. To distinguish between the cases of low reflectivity and those where the low antenna signal is due to the FR, we employ the image autocorrelation analysis. This analysis also helps determine the parameters of the FR, which, in turn, allow us to introduce an approach for correcting the single-polarization SAR images distorted by FR.

Keywords: magnetic field of the Earth, anisotropic ionosphere, propagation of radio waves through gyrotropic plasma, deterioration of radar image, image autocorrelation analysis, evaluation of Faraday rotation effect, correction of the matched filter

(Some figures may appear in colour only in the online journal)

1. Introduction

The Earth's ionosphere may have an adverse effect on spaceborne synthetic aperture radar (SAR) imaging. In our previous work on the subject [1–3], we have shown that this adverse effect is due to the mismatch between the actual radar signal affected by the dispersion of radio waves in the ionospheric plasma, and the matched filter used for signal processing. Accordingly, to improve the image one should correct the filter, which requires knowledge of the total electron content (TEC) in the ionosphere along the signal path. The TEC, in turn, can

be reconstructed by probing the ionosphere on two distinct carrier frequencies and exploiting the resulting redundancy in the data.

Work [1–3] was done under the assumption that the interrogating field is scalar, and that it propagates in an isotropic medium. In reality, however, the electromagnetic field is represented by vector quantities, and the ionospheric plasma is anisotropic due to the magnetic field of the Earth. A particular type of anisotropy introduced in the ionosphere by the magnetic field is known as gyrotropy [4, 5]. It is a particular case of chirality characterized by a spherical real part (as in the case of an isotropic plasma with no external magnetic field) and an antisymmetric imaginary part of the permittivity tensor. The action of the latter on the electric field is equivalent to the cross product with a pseudovector known as the gyration vector; it is parallel to the external magnetic field. Unless the propagation is normal to the magnetic field, the propagation speeds for the left and right circularly polarized transverse electromagnetic waves in a gyrotropic medium will differ, an effect known as double circular refraction [5]. The radar signals usually have linear polarization, which can be represented as a superposition of two waves with opposite circular polarizations. Due to the phase difference between the doubly refracted circularly polarized waves that accumulates over the propagation path, the linearly polarized waves experience a slow rotation of the plane of polarization with distance, a phenomenon called the Faraday rotation (FR) (see appendix B for further detail).

The FR may have both a positive and negative effect on the transionospheric SAR imaging. If the full polarimetric data are available, then one can reconstruct the FR angle for the radar pulse round-trip between the antenna on the orbit and the target on the ground. The latter, in turn, can be used to obtain the TEC, see, e.g., [6–10] and [11, section 10.4], although the resulting value of the TEC will be subject to ambiguities in the FR angle that can only be determined up to a constant multiple of 2π. If the full polarimetric data are not available, then, according to [7, 8], an explicit *a priori* estimate of the FR is required for understanding how the ionosphere affects the image. For single-polarization imaging, the FR yields an additional mismatch between the received signal and the filter. This mismatch can cause an adverse effect if, e.g., the returned linear polarization is (nearly) perpendicular to the emitted polarization, and hence perpendicular to the field direction that the antenna can receive efficiently. This scenario is by no means impossible, because the rotation angle in the P-band[4] can be quite large.

Even if the emitted and received polarizations are not close to perpendicular, the FR may still be detrimental for imaging. Indeed, the rotation angle may vary substantially along the radar chirp, in which case one can qualitatively think of the received signal as 'twisted.' This happens, in particular, when the carrier frequency is low (P-band) and the bandwidth is high (for better resolution). To the best of our knowledge, the twisting phenomenon has not received any attention in the previous studies of the FR for SAR, see [6–11]. It is, however, very important, as it can cause substantial image artifacts, such as split intensity peaks, see section 5.

In the current paper, we use the image autocorrelation analysis to quantify the effect of the FR on a single-polarization spaceborne SAR image, and correct for the corresponding distortions. The presentation is organized as follows.

A brief exposition of the SAR ambiguity theory is given in section 2. Section 3 describes the modification of the radar ambiguity function due to the FR. In sections 4 and 5, we discuss

[4] P-band is a range of frequencies between 0.25 and 0.5 GHz, or, equivalently, a range of wavelengths between 0.6 and 1.2 m, that partially overlaps with the VHF (0.03–0.3 GHz, or 1–10 m) and UHF (0.3–1 GHz, or 0.3–1 m) bands, see [12, 13]. P-band may be of interest for a number of SAR applications that require, say, some ground and/or foliage penetration. For example, the future ESA's Earth Explorer SAR satellite, called BIOMASS, will operate at 435 MHz [14], which is in P-band. To the best of our knowledge, no civilian SAR satellite is currently in service that operates in P-band or below.

how one can use the information from a given SAR image in order to detect the FR and characterize its variation over the frequency band of the radar. Subsequently, the SAR filter can be corrected to match the actual received signal in the presence of the FR and thus improve the quality of the image (section 6). Section 7 provides a summary (including all essential assumptions) and suggests directions of further research. A number of lengthy derivations have been moved to appendices. Specifically, the factorization of the SAR ambiguity function is considered in appendix A; the FR of a chirped signal is analyzed in appendix B; and the properties of the SAR ambiguity function in the presence of both the dispersion and FR are studied in appendices C and D.

2. SAR ambiguity theory

The exposition in this section draws upon [15, 16]. We present this material because it establishes a foundation for section 3 where the key analysis of our study is done.

Let us first assume that the propagation is undistorted, i.e., that there is no plasma and no FR. The evolution of a scalar field $\varphi(t, z)$ is governed by the d'Alembert equation:

$$\left(\frac{1}{c^2}\frac{\partial^2}{\partial t^2} - \Delta\right)\varphi(t, z) = F(t, z), \tag{1}$$

where c is the speed of light, $F(t, z)$ is the source term (its relation to the antenna current can be found in [15, 17]), and boldface symbols ($\boldsymbol{z}$, $\boldsymbol{x}$, etc.) denote points in a stationary three-dimensional frame of reference. For an unsteady point source at $\boldsymbol{x}$:

$$F(t, z) = P(t)\delta(z - \boldsymbol{x}), \tag{2}$$

the solution of (1) is given by the standard retarded potential:

$$\varphi(t, z) = \frac{1}{4\pi}\frac{P(t - |z - \boldsymbol{x}|/c)}{|z - \boldsymbol{x}|}. \tag{3}$$

Hereafter, we will assume that the time dependence $P(t)$ in (2) corresponds to a linear upchirp with the central frequency ω_0:

$$P(t) = A(t)\,\mathrm{e}^{\mathrm{i}\omega_0 t}, \quad \text{where} \quad A(t) = \chi_\tau(t)\,\mathrm{e}^{\mathrm{i}\alpha t^2} \tag{4}$$

and

$$\chi_\tau(t) = \begin{cases} 1, & t \in [-\tau/2, \tau/2], \\ 0, & \text{otherwise.} \end{cases} \tag{5}$$

In formula (4), $\alpha = \frac{B}{2\tau}$ is the chirp rate, $\frac{B}{2\pi}$ is the bandwidth of the chirp, and τ is its duration; these quantities are the constants that define the interrogating waveform. The instantaneous frequency ω is thus a linear function of time:

$$\omega(t) = \omega_0 + 2\alpha t \quad \text{for} \quad t \in [-\tau/2, \tau/2] \tag{6}$$

that varies in the interval of $[\omega_0 - B/2, \omega_0 + B/2]$. It should be noted that formulas (4)–(5) describe a rectangular chirp, while in practice, smoother pulse envelopes are used in order to reduce sidelobes [18, section 2.6]. We use the chirp (4)–(5) because it yields more compact formulae later on, including the well-known sinc-type point spread functions (PSFs) in (17)–(19), but analysis for windowed pulses is also possible.

Let $n = n(z)$ be the local index of refraction and

$$\nu(z) = \frac{1 - n^2(z)}{c^2} \tag{7}$$

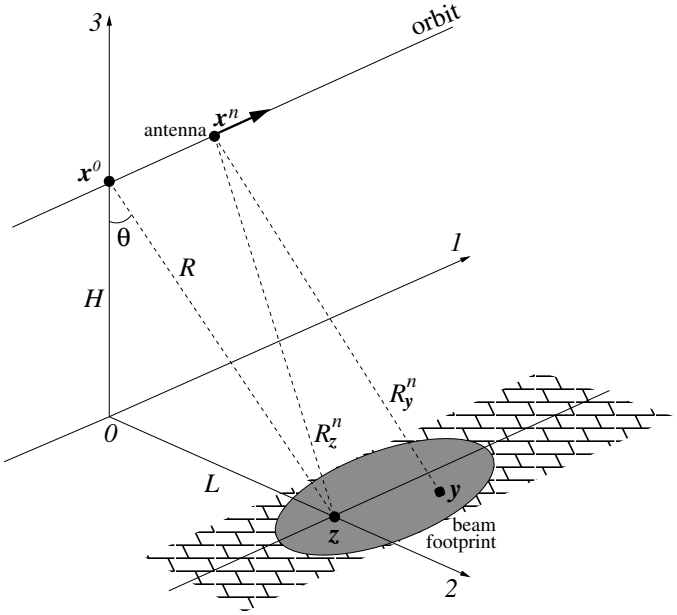

Figure 1. Schematic for the broadside stripmap SAR imaging.

be the ground reflectivity function. For the signal (4) emitted from $\boldsymbol{x}$ and propagating according to (3), the first Born approximation [19, section 13.1.4] yields the following scattered field at the same location $\boldsymbol{x}$:

$$\psi(t,\boldsymbol{x}) \approx \int \tilde{\nu}(\boldsymbol{x},\boldsymbol{z}) P\left(t-2|\boldsymbol{x}-\boldsymbol{z}|/c\right) \mathrm{d}^3\boldsymbol{z}, \tag{8}$$

where

$$\tilde{\nu}(\boldsymbol{x},\boldsymbol{z}) = -\frac{\omega_0^2}{16\pi^2}\frac{\nu(\boldsymbol{z})}{|\boldsymbol{x}-\boldsymbol{z}|^2}. \tag{9}$$

The SAR image is obtained by applying the matched filter $\overline{P(t-2|\boldsymbol{x}-\boldsymbol{y}|/c)}$ to the received antenna signal (8):

$$\begin{aligned} I(\boldsymbol{y}) &= \int_\chi \overline{P(t-2|\boldsymbol{x}-\boldsymbol{y}|/c)}\,\psi(t,\boldsymbol{x})\,\mathrm{d}t \\ &= \int \mathrm{d}^3\boldsymbol{z}\,\tilde{\nu}(\boldsymbol{x},\boldsymbol{z}) \underbrace{\int_\chi \overline{P(t-2|\boldsymbol{x}-\boldsymbol{y}|/c)} P(t-2|\boldsymbol{x}-\boldsymbol{z}|/c)\,\mathrm{d}t}_{W(\boldsymbol{y},\boldsymbol{z})}. \end{aligned} \tag{10}$$

In formula (10), the overbar denotes complex conjugation, the interior integral $W(\boldsymbol{y},\boldsymbol{z})$ is the PSF[5], and the notation $\int_\chi$ means that the integration limits are determined by the indicator function(s) χ_τ under the integral, see (4) and (5). Henceforth, $\boldsymbol{y}$ and $\boldsymbol{z}$ will always be used as 'image coordinate' and 'target coordinate', respectively.

Next, consider a sequence of equally spaced radar pulses, each emitted at the time t^n from the position $\boldsymbol{x}^n$, $n \in [-N/2, N/2]$, see figure 1. Here, N is the number of pulses in the

[5] Oftentimes, the PSF $W(\boldsymbol{y},\boldsymbol{z}_0)$ is interpreted as the image $I(\boldsymbol{y})$ of a point target $\tilde{\nu}(\boldsymbol{x},\boldsymbol{z}) \sim \delta(\boldsymbol{z}-\boldsymbol{z}_0)$, with $\boldsymbol{z}_0$ as a parameter.

synthetic aperture, which is a sliding interval of the antenna track equal in length or shorter than the longitudinal dimension of the beam footprint on the ground. We will use the lower indices 1 and 2 to denote the azimuthal (along the track) and range (normal to the track) horizontal coordinates, respectively, and assume that $z_1 = 0$. For the image $I(\boldsymbol{y})$ given by a coherent sum of expressions (10) for $t = t^n$, $\boldsymbol{x} = \boldsymbol{x}^n$, $W(\boldsymbol{y}, z)$ is replaced by the sum of individual contributions:

$$W(\boldsymbol{y}, z) = \sum_{n=-N/2}^{N/2} W^n(\boldsymbol{y}, z). \tag{11}$$

Each term in the sum (11) is defined as the interior integral in (10):

$$W^n(\boldsymbol{y}, z) = \int_\chi \overline{P\big(u_y^n\big)} P\big(u_z^n\big)\, \mathrm{d}t, \tag{12}$$

where

$$u_y^n = t - t^n - 2R_y^n/c, \quad u_z^n = t - t^n - 2R_z^n/c, \quad \text{and} \quad R_y^n = |\boldsymbol{y} - \boldsymbol{x}^n|, \quad R_z^n = |z - \boldsymbol{x}^n|. \tag{13}$$

The sum (11) is called the generalized ambiguity function (GAF) of the SAR. The constant t^n in (12)–(13) can be removed by changing the integration variable (shifting). Then, noticing that the dependence of $\overline{A(u_y^n)}$ and $A(u_z^n)$ on n is through $\boldsymbol{x}^n$ and is therefore weak, we can pull these terms out of the summation over n, so that the GAF (11) can be factorized (see [2, 3, 15, 16]):

$$W(\boldsymbol{y}, z) \approx W_A(\boldsymbol{y}, z) \cdot W_R(\boldsymbol{y}, z). \tag{14}$$

In formula (14),

$$W_A(\boldsymbol{y}, z) = \sum_{n=-N/2}^{N/2} \mathrm{e}^{2\mathrm{i}\omega_0 (R_y^n - R_z^n)/c}, \tag{15}$$

$$W_R(\boldsymbol{y}, z) = \int_\chi \overline{A\big(u_y^0\big)} A\big(u_z^0\big)\, \mathrm{d}t, \tag{16}$$

and the superscript '0' refers to formulae (13) for $\boldsymbol{x} = \boldsymbol{x}^0$. We emphasize that representation (14)–(16) is only approximate. The error of the factorization is analyzed in appendix A and is shown to be small, of the order of $\frac{B}{\omega_0}$, see formula (A.19). Moreover, this error becomes even smaller (insignificant) if the target z and the reference point $\boldsymbol{y}$ have either the same range coordinate or the same azimuthal coordinate.

The actual calculation of the range and azimuthal factors of the GAF (15) and (16) is also done in appendix A. In particular, the azimuthal factor (15) evaluates to

$$\begin{aligned} &W_A(\boldsymbol{y}, z) \approx \mathrm{e}^{\mathrm{i}\Phi_0} N \operatorname{sinc}\left(\pi \frac{y_1}{\Delta_A}\right), \\ &\text{where} \quad \Phi_0 = 2\frac{\omega_0\big(R_y^0 - R_z^0\big)}{c} \quad \text{and} \quad \Delta_A = \frac{\pi R c}{\omega_0 L_{\mathrm{SA}}}. \end{aligned} \tag{17}$$

The quantity Δ_A in (17) is the azimuthal resolution; it depends, in particular, on the distance R between the target z and the orbit, see figure 1, as well as on the length of the synthetic aperture L_{SA}, which can be 10 km or greater for spaceborne SAR applications. The sinc function in (17) defines the shape of the GAF in the azimuthal direction.

Remark. The quantity $\mathrm{e}^{\mathrm{i}\Phi_0}$ in W_A, see (17), is a factor of magnitude one in front of the sum. It may not have received proper attention in the earlier accounts of the SAR ambiguity theory, including those of our own [1–3]. This factor rapidly oscillates in range. While an

inconvenience at a first glance, it actually helps redefine the ground reflectivity function so that to enable backscattering via the Bragg mechanism. The corresponding analysis, however, is quite involved and goes well beyond the scope of the current work; it will be presented elsewhere. Hereafter, we merely disregard the rapidly oscillating factor $e^{i\Phi_0}$, which means that $\nu(z)$ needs to be interpreted as the local backscattering coefficient at the target rather than the plain variation of the refraction index, as in (7).

Remark. The geometrical spreading of spherical waves, which is accounted for by the denominator in formula (9), can also be included into the definition of the ground reflectivity. Indeed, for $\boldsymbol{x}$ within a given synthetic aperture, the denominator of (9) varies slowly and produces only insignificant changes in the signal amplitude. Therefore, for the rest of the current paper we will disregard the dependence of $\tilde{\nu}$ on $\boldsymbol{x}$ in (9).

The range factor W_R of (16) is expressed as

$$W_R(\boldsymbol{y},\boldsymbol{z}) \approx \tau\, w_p(\xi) \equiv \tau\, w_p\left(\pi\,\frac{R_y^0 - R_z^0}{\Delta_R}\right), \qquad \text{where} \quad \Delta_R = \frac{\pi c}{B}. \tag{18}$$

The quantity Δ_R in formula (18) is the range resolution, and

$$\begin{aligned} w_p(\xi) &= \frac{1}{\tau}\int_\chi \overline{A(u_y^0)}A(u_z^0)\,\mathrm{d}t \approx \frac{1}{\tau}\int_{-\tau/2}^{\tau/2} e^{ibu}\,\mathrm{d}u = \operatorname{sinc}\xi, \\ b &= \frac{4\alpha(R_y^0 - R_z^0)}{c}, \qquad \xi = \frac{b\tau}{2} = \pi\,\frac{R_y^0 - R_z^0}{\Delta_R} \approx \pi\,\frac{(y_2 - z_2)\sin\theta}{\Delta_R}. \end{aligned} \tag{19}$$

The function $w_p(\xi)$ of (19) defines the shape of the GAF in the range direction.

Remark. In formula (19) (as well as in (32) below), we use $\pm\tau/2$ as the integration limits. In appendix A, more accurate expressions for these limits are introduced: $\pm\tau^0/2$, where $\tau^0 = \tau - 2|R_y^0 - R_z^0|/c$ (see formulae (A.4)–(A.5)). Since for the high range resolution chirp we are assuming $B\tau \gg 1$ [18, 20], one can show that

$$\frac{|\tau - \tau^0|}{\tau} = \frac{2\left|R_y^0 - R_z^0\right|}{c\tau} \sim \frac{\Delta_R}{c\tau} = \frac{\pi}{B\tau} \ll 1,$$

so the difference is insignificant.

3. Ambiguity function in the presence of the Faraday rotation

The propagation of radar signals in the ionospheric plasma affects the SAR imaging in two ways. First, the temporal dispersion of radio waves alters the envelope and phase of the received signal, see [1–3]. Second, the magnetic field of the Earth causes the FR, see [4, 7, 21]. These distortions, if not accompanied by the proper corrections of the filter, lead to image deterioration due to the filter mismatch.

In appendix B, we consider the effect of the FR on the chirped signals. For an antenna operating on a single linear polarization, the effective antenna signal in the presence of the rotation is related to the non-rotated signal $\psi(t,\boldsymbol{x})$ of (8) as

$$\psi_F(t,\boldsymbol{x}) = \psi(t,\boldsymbol{x})\cos\varphi_F(\omega), \tag{20}$$

where φ_F is the rotation angle (see the top row of (B.19)), and $\psi(t,\boldsymbol{x})$ is the signal amplitude for the isotropic case, see (8). An important assumption we make here is that the target reflectivity $\nu(z)$ given by (7) is independent on the polarization of the incident field. More realistic scattering models may be used in the approach we develop below; however, the interpretation of results will be more involved, and we leave this for future work.

For the two-way propagation in a magnetized plasma, the angle φ_F depends on the instantaneous frequency as (see also (B.20)):

$$\varphi_F(\omega) = 2 \cdot \frac{R}{2c} \frac{\omega_{pe}^2 \Omega_e \cos\beta}{\omega^2} \propto \omega^{-2}, \tag{21}$$

where R is the distance from the target to the orbit (300–1000 km), ω_{pe} is the Langmuir frequency, Ω_e is the electron cyclotron frequency, and β is the angle between the ray path and the magnetic field. Formula (21) shows that the low frequency and high frequency parts of the chirp (4) will be rotated by different angles and, according to (20), their amplitudes will be reduced by different factors when received by the antenna.

Remark. For the actual ionosphere, the quantity $\omega_{pe}^2 \Omega_e \cos\beta$ in (21) should be averaged over the ray path. The value of $\int \omega_{pe}^2 \Omega_e \cos\beta \, ds$ along the ray path is an integral characteristic of the propagation through a magnetized plasma. It determines the difference of eikonals for two waves with opposite circular polarizations. For the FR, it plays the same role as the TEC plays for dispersion-related distortions [2, 3, 22]. The TEC is given by the integral $\int n_e \, ds \propto \int \omega_{pe}^2 \, ds$, see (B.3). It yields the variation of the eikonal due to the temporal dispersion.

Next, we approximate $\cos\varphi_F$ in (20) by the first two terms of its Taylor expansion w.r.t. $u = t - 2R/c$, and, using (6), obtain:

$$\cos\varphi_F(u) \equiv \cos\varphi_F(\omega(u)) \approx p + \frac{2q}{\tau} u, \tag{22}$$

where

$$\begin{aligned} p &= \cos\varphi_F(\omega_0), \\ q &= \frac{\tau}{2} \frac{d\cos\varphi_F}{du}(\omega_0) = -\frac{\tau}{2} \sin\varphi_F \frac{d\varphi_F}{d\omega} \frac{d\omega}{du}(\omega_0) \\ &\approx \frac{BR}{c} \frac{\omega_{pe}^2 \Omega_e \cos\beta}{\omega_0^3} \sin\varphi_F(\omega_0) = \frac{B}{\omega_0} \varphi_F(\omega_0) \sin\varphi_F(\omega_0). \end{aligned} \tag{23}$$

Thus, the FR manifests itself by an additional reduction of the signal amplitude received by the antenna, with the reduction coefficient, $\cos\varphi_F$, varying over the chirp (see (20) and (22)). Two non-dimensional constants, p and q, are introduced in (22), (23) to describe this effect. If we take the amplitude of the non-rotated antenna signal as 1, then, with the FR present, the amplitude at the center of the chirp is p, while the end-to-end variation over the chirp is $2q$. We have $|p| \leqslant 1$ by definition, and $|q| \ll 1$ as a condition of applicability of the Taylor linearization, see (22).

Remark. Linear approximation (22) will be in the core of our subsequent analysis. Of course, its use may be justified only if the variation of $\cos\varphi_F$ over the chirp is small, i.e., $|q| \ll 1$. The FR angle for $\omega_0/2\pi \lesssim 0.5$ GHz may reach $\pi/2$ for ionospheric propagation, see [21]. Taking $B/\omega_0 \sim 5\%$, we get from (22) about $0.1 \cdot \pi/2$ variation of the FR angle over the chirp, which we consider sufficiently small for linearization. Thus, the validity of a linearization-based approach depends on the system parameters, such as central frequency and bandwidth, as well as on the propagation parameters (TEC and strength and direction of magnetic field, see (23)). In particular, the linearization may fail for broadband systems where variations of $\cos\varphi_F$ is large (see case (c) in section 4 below).

As mentioned in section 1, the cause of the FR is double circular refraction in a gyrotropic medium [5, chapter XI], which results in different propagation speeds for two circular waves that form the original linear polarization, see also appendix B for detail. In the dispersive yet rotation-less case [1–3], correcting the filter for dispersive effects helps remove the

corresponding image distortions, and the expression for the GAF becomes similar to that for the non-dispersive case. In appendix C, we show that in the presence of both the dispersion and gyrotropy, such a filter will still eliminate the dispersion-related part of distortions, leaving the rotation effect intact. For that reason, hereafter we assume that the FR accompanies a plain non-dispersive propagation of the radar signals. In a comprehensive setting, this means that the compensation of the FR in the SAR filter discussed in section 6 should be applied on top of the dispersion correction.

In the presence of the FR, the imaging formula (10) transforms into

$$\begin{aligned} I_F(\boldsymbol{y}) &= \int_\chi \overline{P(t-2|\boldsymbol{x}-\boldsymbol{y}|/c)}\psi_F(t,\boldsymbol{x})\,\mathrm{d}t \\ &= \int \tilde{\nu}(z) W_F(\boldsymbol{y},z)\,\mathrm{d}^3 z, \end{aligned} \tag{24}$$

where $\psi_F(t,\boldsymbol{x})$ is given by (20) and the kernel $W_F(\boldsymbol{y},z)$ takes into account (22):

$$\begin{aligned} W_F(\boldsymbol{y},z) &= \int_\chi \overline{P(u_y)}P(u_z)\cos\varphi_F(u_z)\,\mathrm{d}t \\ &= pW(\boldsymbol{y},z) + q\frac{2}{\tau}W_q(\boldsymbol{y},z). \end{aligned} \tag{25}$$

In formula (25), $W(\boldsymbol{y},z)$ coincides with that of (10), and

$$W_q(\boldsymbol{y},z) = \int_\chi \overline{P(u_y)}u_z P(u_z)\,\mathrm{d}t. \tag{26}$$

Remark. Henceforth, we will be using the subscript 'q' to denote contributions due to the FR, as in (26); in the isotropic case (i.e., when there is no magnetic field), these terms vanish. The subscript 'F' will be used to denote the characteristics affected by the FR, i.e., having both rotational and non-rotational 'components,' as on the left-hand side of (25); in the isotropic case, these expressions reduce to their isotropic counterparts, e.g., $W_F(\boldsymbol{y},z)$ in (25) reduces to $W(\boldsymbol{y},z)$ in (10).

For the sequence of emitted and received signals, definition (11) is replaced by (C.5) with primes dropped:

$$W_F(\boldsymbol{y},z) = \sum_{n=-N/2}^{N/2} W_F^n(\boldsymbol{y},z), \tag{27}$$

where $W_F^n(\boldsymbol{y},z)$ is given by the first line of (25). Using approximation (22), we can write:

$$W_F^n(\boldsymbol{y},z) = pW^n(\boldsymbol{y},z) + q\frac{2}{\tau}\int_\chi \overline{P\big(u_y^n\big)}u_z^n P\big(u_z^n\big)\,\mathrm{d}t, \tag{28}$$

where $W^n(\boldsymbol{y},z)$ is the same as in (12). An approximate factorization of the GAF (27), (28) similar to (14) is also possible:

$$W_F(\boldsymbol{y},z) \approx W_A(\boldsymbol{y},z)\cdot W_{RF}(\boldsymbol{y},z), \tag{29}$$

where the azimuthal factor $W_A(\boldsymbol{y},z)$ does not change and is still defined by (15), and

$$W_{RF}(\boldsymbol{y},z) = pW_R(\boldsymbol{y},z) + q\frac{2}{\tau}W_{qR}(\boldsymbol{y},z). \tag{30}$$

In formula (30), $W_R(\boldsymbol{y},z)$ is given by (16), and

$$W_{qR}(\boldsymbol{y},z) = \int_\chi \overline{A\big(u_y^0\big)}u_z^0 A\big(u_z^0\big)\,\mathrm{d}t. \tag{31}$$

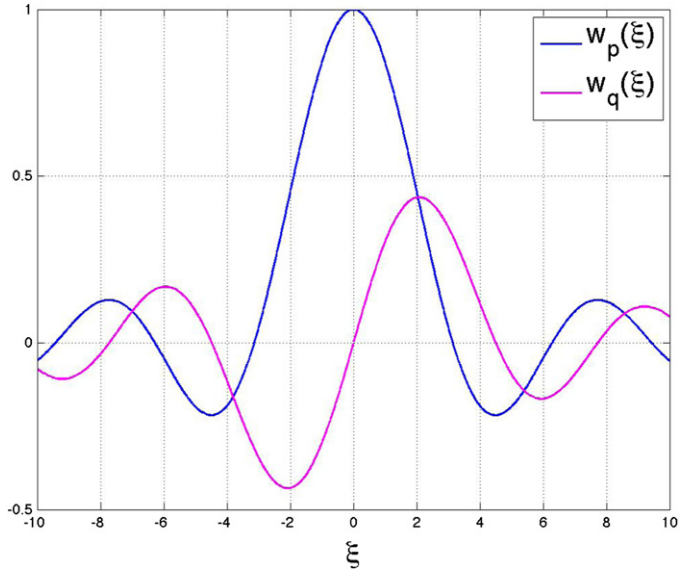

Figure 2. Components of the range factor (33) in the presence of the Faraday rotation.

Thus, the FR results in a modification of the range factor in the approximate formula (29) compared to (14): $W_{RF}(\boldsymbol{y},\boldsymbol{z})$ of (30), (31) replaces $W_R(\boldsymbol{y},\boldsymbol{z})$ of (16). It is shown in appendix D that the error due to the factorization (29) is small—of the same order as that for (14), i.e., about $\frac{B}{\omega_0}$, see formula (D.5).

Introducing a new dimensionless function

$$w_q(\xi) \stackrel{\text{def}}{=} \frac{2}{\mathrm{i}\tau^2}\int_{\chi}\overline{A\big(u_y^0\big)}u_z^0 A\big(u_z^0\big)\,\mathrm{d}t \approx \frac{2}{\mathrm{i}\tau^2}\int_{-\tau/2}^{\tau/2} u\,\mathrm{e}^{\mathrm{i}bu}\,\mathrm{d}u$$
$$= \frac{2}{\tau^2}\frac{1}{\mathrm{i}^2}\frac{\mathrm{d}}{\mathrm{d}b}\int_{-\tau/2}^{\tau/2}\mathrm{e}^{\mathrm{i}bu}\,\mathrm{d}u = -\frac{\mathrm{d}}{\mathrm{d}\xi}w_p(\xi) = -w_p'(\xi), \tag{32}$$

we can represent W_{RF} of (30) as

$$W_{RF}(\boldsymbol{y},\boldsymbol{z}) = W_{RF}(\xi) = \tau\left(pw_p(\xi) + \mathrm{i}qw_q(\xi)\right), \tag{33}$$

where w_p, b, and ξ are given by (19).

Remark. When integrating in (32), we have replaced τ^0 with τ, similarly to how we did it for w_p, see formula (19) and the subsequent remark. This introduces a small error. The formulae with no simplification can be found in appendix D, see (D.4).

4. Detection of the Faraday rotation

The FR affects the GAF $W_F(\boldsymbol{y},\boldsymbol{z})$ via the range factor (33). It is to be noted that while the real part of the range ambiguity function W_{RF} in (33) is an even function of its argument, see (19), the imaginary part is proportional to $w_q = -w_p'$ and is therefore an odd function, see figure 2 (the singularity of w_q at $\xi = 0$ is removable by setting $w_q(0) = 0$). As far as the relative contribution of w_p and w_q into W_{RF}, there are several qualitatively different regimes determined by the range of variation of the amplitude reduction coefficient $\cos\varphi_F$ over the bandwidth, see (22).

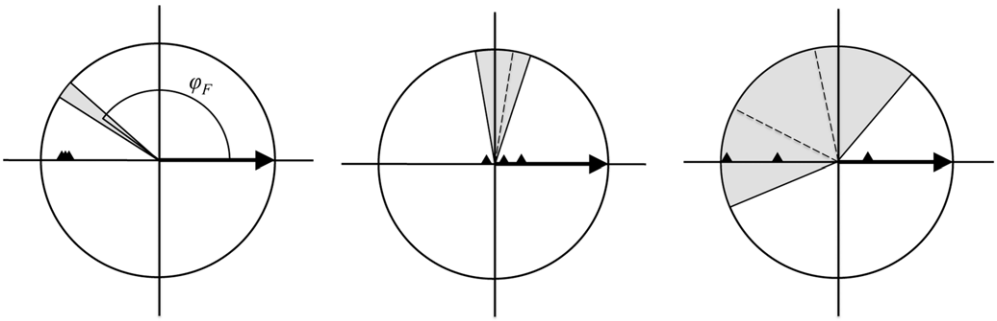

(a) Narrow range of φ_F (b) Intermediate range of φ_F (c) Wide range of φ_F

Figure 3. Examples of possible ranges of φ_F for the chirp propagating through a gyrotropic medium shown in a plane normal to the direction of propagation. The thick arrow indicates the polarization of the emitted field. The ranges for φ_F for $B/3$ sub-bands are shown by dashed lines according to (22), while the values of $\cos\varphi_F$ averaged over the sub-bands are indicated by triangles on the horizontal axis.

(a) $|q| \ll |p|$. This is the case of nearly uniform amplitude reduction where all possible φ_Fs lie in a narrow range of angles, see figure 3(a). In essence, it is this case that has been previously assumed in the literature when studying the FR for SAR applications [6–11]. As the relative contribution of w_q is small, the correction for the FR is not necessary. This is also the case where the detection of the FR by a single-polarization instrument is difficult.

(b) $|p| \lesssim |q|$. The case of an intermediate range of φ_F, see figure 3(b), that presents a challenge—the image is both reduced in intensity and distorted by the FR; yet if $p \neq 0$, the 'double peak' feature of $w_q(\xi)$ is smeared out by the $pw_p(\xi)$ term in (33) and may not be easily observable.

(c) $|q| \gtrsim 1$. The range of φ_F is wide, see figure 3(c), which is the opposite to case (a). The correction is required; however, the linearization of $\cos\varphi_F(u)$ in (22) is not valid. We do not consider this case hereafter.

The foregoing three cases can be very roughly discriminated by means of the sub-band processing. Assume that the entire bandwidth B of the signal is split, say, into three sub-bands of bandwidth $B/3$ each. The average of $\cos\varphi_F$ over a sub-band will be approximately the same for all sub-bands for case (a) and will vary substantially from one sub-band to another for cases (b) and (c), see figure 3. Lower resolution images can be obtained by sub-band processing [3, appendix D], and a substantial variation between their intensities can be indicative of the presence of a significant FR.

All subsequent analysis in this paper applies primarily to the intermediate case (b).

5. Evaluation of the Faraday rotation effect

In this section (unlike in section 4), we will be using a single full-band image to calculate the parameters that characterize the FR.

If the reflectivity of the target is not known, then in the problem of reconstruction of the FR parameters from the image I_F we have one equation (cf (10)):

$$I_F(\mathbf{y}) = \int W_F(\mathbf{y}, z)\tilde{\nu}(z)\,\mathrm{d}^3 z \tag{34}$$

with two unknowns: W_F of (29) and $\tilde{\nu}$. The information about the FR is contained in W_F, but in order to retrieve this information from (34), we should make certain assumptions about the other unknown, i.e., $\tilde{\nu}$. Specifically, we adopt the model of a homogeneous distributed scatterer[6] for $\tilde{\nu}(z)$, and subsequently employ the image autocorrelation analysis. Our goal is to find the parameters p and q that characterize the FR, see (22) and (30). It turns out that only the ratio of those parameters can be obtained, but it proves sufficient to correct the filter, see section 6.

We first notice that imaging in azimuth is not affected by the FR, see (14) and (29), (30). Hence, we can exploit the decoupling between azimuth and range due to the factorization of the GAF. In other words, we can process the image in azimuth ahead of time and subsequently focus on the one-dimensional imaging with respect to the range coordinate only. To do so, we recast (34) (with the account of the remark preceding equation (18)) as

$$I(y_1, y_2) = \int_{-\infty}^{\infty}\int_{-\infty}^{\infty} W_A(y_1, z_1) W_{RF}\big(R_y^0, R_z^0\big)\tilde{\nu}(z_1, z_2)\,\mathrm{d}z_1\,\mathrm{d}z_2, \tag{35}$$

where W_A is given by (15), (17), W_{RF} is given by (16), (30), (31), and the arguments of W_A and W_{RF} in (35) emphasize their dependence on the azimuthal and range variables, respectively (see coordinate notations in figure 1). We also assume that the function $\tilde{\nu}(z_1, z_2)$ in (35) already accounts for the transition from the volumetric reflectivity $\tilde{\nu}(\boldsymbol{z}) \equiv \tilde{\nu}(z_1, z_2, z_3)$ to the single layer $\tilde{\nu}(z_1, z_2)\delta(z_3)$ on the surface $z_3 = 0$, see [23, section 3].

The difference $R_y^0 - R_z^0$, which enters the argument of W_{RF} via (19) and (33), does not depend on either y_1 or z_1, see formula (A.11) for $x_1^n = 0$. Therefore, equation (35) transforms into:

$$I(y_1, y_2) = \int_{-\infty}^{\infty} W_{RF}(y_2, z_2) \underbrace{\int_{-\infty}^{\infty} W_A(y_1, z_1)\tilde{\nu}(z_1, z_2)\,\mathrm{d}z_1}_{\nu_R(y_1, z_2)}\,\mathrm{d}z_2, \tag{36}$$

where $\nu_R(y_1, z_2)$ is already an image in the azimuthal direction, but still retains the meaning of a ground reflectivity in the range direction. Equation (36) can be considered independently for each y_1, which effectively implies one-dimensional imaging in range only. As such, we will henceforth use the plain non-indexed variables (y, z) instead of (y_2, z_2), and also drop y_1 from the arguments of I and ν_R. Then, formula (36) yields:

$$I(y) = \int_{-\infty}^{\infty} W_{RF}(y, z)\nu_R(z)\,\mathrm{d}z, \tag{37}$$

where W_{RF} is, in fact, a single variable function: $W_{RF} = W_{RF}(y - z)$, see (19), (33).

To model a homogeneous distributed scatterer, we assume that $\nu_R(z)$ has a rapidly decaying autocorrelation function (ACF) that we approximate by the delta function:

$$V_\nu(z) \overset{\text{def}}{=} \int_{-\infty}^{\infty} \nu_R(y - z)\bar{\nu}_R(y)\,\mathrm{d}y \approx \sigma^2\delta(z). \tag{38}$$

The quantity σ^2 in formula (38) is the average backscattering intensity. The approximation in (38) shall be understood in the sense of distributions, so that for any appropriate test function $\phi(z)$ we have $\int V_\nu(z)\phi(z)\,\mathrm{d}z \approx \sigma^2\phi(0)$. Relation (38) is helpful in that it greatly simplifies the analysis; besides, it is routinely used in the literature dealing with radar speckle to model the so-called uniform extended targets, see, e.g., [24–27], [11, section 4.4], [28, chapters 4, 5],

[6] Alternatively, one can use point scatterers: $\tilde{\nu}(\boldsymbol{z}) = \sum_m \nu_m\delta(\boldsymbol{z} - \boldsymbol{z}_m)$ so that (34) yields: $I_F(\boldsymbol{y}) = \sum_m \nu_m W_F(\boldsymbol{y}, \boldsymbol{z}_m)$. Considering $I_F(\boldsymbol{y})$ at sufficiently many reference locations $\boldsymbol{y}$ as given data, and taking into account that w_p and w_q in (33) are known analytically, one can obtain an overdetermined system of equations and solve it in a weak sense with respect to p and q. In a practical setting, however, the problem with dominant point scatterers is their availability. That's why we subsequently focus on the approach suitable for distributed scatterers.

and [29, section 3.11]. More sophisticated models for reflectivity autocorrelation may be required to describe other types of targets, see, e.g., [28, chapter 9].

With the help of (38), we can easily compute the ACF of the image $I(y)$ of (37):

$$\begin{aligned}\int_{-\infty}^{\infty} I(y)\bar{I}(y+h)\,\mathrm{d}y &= \int_{-\infty}^{\infty}\int_{-\infty}^{\infty} W_{RF}(y-z)\nu_R(z)\,\mathrm{d}z\int_{-\infty}^{\infty}\bar{W}_{RF}(y+h-z')\bar{\nu}_R(z')\,\mathrm{d}z'\,\mathrm{d}y\\ &= \int_{-\infty}^{\infty}\int_{-\infty}^{\infty} W_{RF}(z)\nu_R(y-z)\,\mathrm{d}z\int_{-\infty}^{\infty}\bar{W}_{RF}(z'+h)\bar{\nu}_R(y-z')\,\mathrm{d}z'\,\mathrm{d}y\\ &= \iiint_{-\infty}^{\infty} W_{RF}(z)\bar{W}_{RF}(z'+h)\nu_R(y-z)\bar{\nu}_R(y-z')\,\mathrm{d}z\,\mathrm{d}z'\,\mathrm{d}y\\ &= \iint_{-\infty}^{\infty} W_{RF}(z)\bar{W}_{RF}(z'+h)\int_{-\infty}^{\infty}\nu_R(y-z)\bar{\nu}_R(y-z')\,\mathrm{d}y\,\mathrm{d}z\,\mathrm{d}z'\\ &= \iint_{-\infty}^{\infty} W_{RF}(z)\bar{W}_{RF}(z'+h)V_\nu(z-z')\,\mathrm{d}z\,\mathrm{d}z'\\ &= \sigma^2\int_{-\infty}^{\infty} W_{RF}(z)\bar{W}_{RF}(z+h)\,\mathrm{d}z. \end{aligned}\tag{39}$$

The final step in (39) is made using (38). As W_{RF} is a smooth function with a characteristic scale of Δ_R, the requirement on the actual scale of V_ν can, perhaps, be relaxed (compared to (38)) to let this scale be finite but much shorter than Δ_R.

Next, introduce a shorthand notation

$$w_1 * w_2 \equiv (w_1 * w_2)(\zeta) \stackrel{\text{def}}{=} \int_{\infty}^{\infty} w_1(\xi)w_2(\xi+\zeta)\,\mathrm{d}\xi,$$

where $w_{1,2}$ denote any of the functions w_p or w_q, and $\zeta = Bh\sin\theta/c$. Then, using (33), we can transform the integral on the right-hand side of (39) as follows:

$$\begin{aligned}&\int_{-\infty}^{\infty} W_{RF}(z)\bar{W}_{RF}(z+h)\,\mathrm{d}z\\ &\qquad = \tau^2\frac{c}{B\sin\theta}(p^2 w_p * w_p + q^2 w_q * w_q + \mathrm{i}pq(w_q * w_p - w_p * w_q)).\end{aligned}\tag{40}$$

Using contour integration on the complex plane, one can show that the function $w_p * w_p$ from (40) takes the form

$$w_p * w_p = \int_{-\infty}^{\infty}\frac{\sin\xi}{\xi}\frac{\sin(\xi+\zeta)}{(\xi+\zeta)}\,\mathrm{d}\xi = \pi\,\mathrm{sinc}\,\zeta,\tag{41a}$$

while for the remaining three terms on the right-hand side of (40), we have:

$$-w_p * w_q = w_q * w_p = \frac{\mathrm{d}}{\mathrm{d}\zeta}(w_p * w_p),\tag{41b}$$

and

$$w_q * w_q = -\frac{\mathrm{d}}{\mathrm{d}\zeta}(w_q * w_p) = -\frac{\mathrm{d}^2}{\mathrm{d}\zeta^2}(w_p * w_p).\tag{41c}$$

Substituting (40)–(41) into (39), we arrive at

$$\int_{-\infty}^{\infty} I(y)\bar{I}(y+h)\,\mathrm{d}y = \pi D\tau^2\frac{c}{B\sin\theta}(\mathrm{sinc}\,\zeta + 2\mathrm{i}Q\,\mathrm{sinc}'\,\zeta - Q^2\,\mathrm{sinc}''\,\zeta),\tag{42}$$

where

$$D = p^2\sigma^2 \quad \text{and} \quad Q = \frac{q}{p}.\tag{43}$$

The left-hand side of equation (42) represents the data. For brevity, let us denote

$$\int_{-\infty}^{\infty} I(y)\bar{I}(y+h)\,\mathrm{d}y = g(h). \tag{44}$$

For a given h, the ACF $g(h)$ can be evaluated directly from the image, although in practice the integration limits are, of course, finite[7].

The right-hand side of equation (42) is a polynomial with respect to the unknown quantities D and Q given by formulae (43). The coefficients of this polynomial are functions of h defined by analytic expressions, because $\zeta = Bh\sin\theta/c$. Let us take two different values of h, $h_1 \neq h_2$, and denote

$$g(h_1) = g_1, \quad g(h_2) = g_2, \quad \zeta(h_1) = \zeta_1, \quad \text{and} \quad \zeta(h_2) = \zeta_2. \tag{45}$$

Then, it is easy to eliminate D from the pair of equations (42) written for h_1 and h_2:

$$(\operatorname{sinc}\zeta_1 + 2iQ\operatorname{sinc}'\zeta_1 - Q^2\operatorname{sinc}''\zeta_1)g_2 = (\operatorname{sinc}\zeta_2 + 2iQ\operatorname{sinc}'\zeta_2 - Q^2\operatorname{sinc}''\zeta_2)g_1. \tag{46}$$

Equation (46) is a plain quadratic equation with respect to Q. It can be solved analytically, after which the value of D can also be obtained, if needed. It doing so, the individual values of p and q can be determined from D and Q only up to a common factor $\sim\frac{1}{\sigma}$. However, knowing their ratio Q proves sufficient for implementing the filter correction, see section 6.

We leave the issue of conditioning of equation (46) for the future study. This study will involve the analysis of sensitivity of its roots to the perturbations of the data g_1 and g_2. As opposed to the values of ζ_1 and ζ_2 of (45) that are known exactly, the data g_1 and g_2 are evaluated from the image by formula (44) with the integration limits replaced by finite quantities. Therefore, g_1 and g_2 may be prone to various inaccuracies which, in turn, will translate into inaccuracies in the determination of Q using equation (46).

However, regardless of a specific quantitative measure of conditioning[8] of equation (46), the final error in the value of Q can be reduced if we obtain multiple estimates $Q^{(k)}$ for $k = 1, 2, \ldots, K$ and then evaluate Q by plain averaging:

$$Q = \frac{1}{K}\sum_{k=1}^{K} Q^{(k)}, \tag{47}$$

which, for the scalar Q, is equivalent to the least squares fit, see [30, chapter 7]. In order to get multiple estimates $Q^{(k)}$, we need multiple pairs of $(g_1^{(k)}, g_2^{(k)})$ to be substituted into equation (46). The latter may come from using multiple uniform patches and/or multiple pairs of (h_1, h_2). Furthermore, several uniform patches with possibly different values of σ^2 could be used because Q does not depend on σ^2, see (43).

Let us now interpret $Q^{(k)}$ obtained from different patches and or different pairs $h_1 \neq h_2$ as independent random variables with means $\langle Q^{(k)}\rangle$ and variances $V^2(Q^{(k)})$, $k = 1, 2, \ldots, K$. Then (see, e.g., [31, chapter 2]),

$$\langle Q\rangle = \frac{1}{K}\sum_{k=1}^{K}\langle Q^{(k)}\rangle \quad \text{and} \quad V^2(Q) = \frac{1}{K^2}\sum_{k=1}^{K} V^2(Q^{(k)}). \tag{48}$$

Assume, in addition, and with no loss of generality, that the errors associated with computing the individual $Q^{(k)}$ are approximately equal to the corresponding standard deviations $V(Q^{(k)})$,

[7] Finite integration limits in formula (44) effectively imply that the quantity $g(h)$ will depend not only on the shift h but also on the location or, rather, area (patch) within the image, across which the integration is performed. This, in turn, means that the quantity σ^2 on the right-hand side of formula (38) can also depend on the patch instead of being interpreted as a constant for the entire image.

[8] High sensitivity of the roots to perturbations of the data implies poor conditioning, while low sensitivity is equivalent to good conditioning, see, e.g., [30, chapter 1].

and that these errors are roughly the same for all $k = 1, 2, \ldots, K$. Then, the second equality in formula (48) indicates that the overall error of evaluating Q according to (47) will decrease proportionally to $K^{-1/2}$ as K increases.

We therefore conclude that robustness of determining the parameters of the FR will increase if multiple equations of type (46) are solved instead of one. We also note that the nature of the perturbations in the data g_1 and g_2 may actually be stochastic if one adopts a statistical interpretation of the target (see, e.g., [25, 26, 28]), for which $\nu_R(z)$ becomes a random field.

6. Reducing image distortions due to the Faraday rotation

In the presence of the FR, the filter $\overline{P(t - 2|\boldsymbol{x} - \boldsymbol{y}|/c)}$ does not match the received signal $\psi_F(t, \boldsymbol{x})$ in (24). The distortions created by this mismatch can be reduced by using the filter $\overline{P_F(t - 2|\boldsymbol{x} - \boldsymbol{y}|/c)}$ that will match $\psi_F(t, \boldsymbol{x})$. The expression for $P_F(t)$ involves the parameter $Q = \frac{q}{p}$ that characterizes the FR (see section 5), and is given by (cf (4))

$$P_F(t) = A_F(t)\mathrm{e}^{\mathrm{i}\omega_0 t}, \quad \text{where} \quad A_F(t) = \chi_\tau(t)\,\mathrm{e}^{\mathrm{i}\alpha t^2}\left(1 + \frac{2Q}{\tau}t\right). \tag{49}$$

Using formulae (20) and (22), the factorization (29), and the corrected filter given by the conjugate of (49), we obtain the following expression for the new range ambiguity function (cf (16) and (30), (31)):

$$\widetilde{W}_{RF}(\boldsymbol{y}, \boldsymbol{z}) = \int_\chi \overline{A_F\big(u_y^0\big)} A\big(u_z^0\big)\left(p + \frac{2q}{\tau}u_z^0\right)\mathrm{d}t. \tag{50}$$

Substituting (13) for $n = 0$ and performing the integration in (50), we get instead of (33):

$$\widetilde{W}_{RF}(\xi) = p\tau((1 + Q^2)w_p(\xi) + 2iQw_q(\xi) - 2Q^2 w_{qq}(\xi)),$$

where the new dimensionless function $w_{qq}(\xi) \stackrel{\text{def}}{=} w_q(\xi)/\xi$ has a removable singularity at $\xi = 0$ if we set $w_{qq}(0) = 1/3$.

To demonstrate the superiority of the corrected ambiguity function $\widetilde{W}_{RF}$ over its unmodified form (33), we plot the corresponding normalized range intensity PSFs

$$\frac{|W_{RF}(\xi)|^2}{\max|W_{RF}|^2} \quad \text{and} \quad \frac{|\widetilde{W}_{RF}(\xi)|^2}{\max|\widetilde{W}_{RF}|^2} \tag{51}$$

for several values of $Q = q/p$, see figure 4. The dashed vertical lines indicate a 3 dB drop of intensity from the maximum. It can be readily seen that the resolution is improved in all cases; however, a more significant improvement is observed for larger Q, as expected.

7. Discussion and future work

In the current paper, we have introduced a mathematical model and analyzed the effect of the FR on single-polarization transionospheric SAR imaging. Unlike in all other studies of the FR in the SAR literature (that exploit either single-polarization or polarimetric framework), our analysis takes into account the variation of the rotation angle along the interrogating chirp, and offers a venue for correcting the matched filter in those cases where the impact of the FR on the image is deemed detrimental. Specifically, we first propose an approach to rough detection of the FR based on sub-band image processing. Then, we employ the image autocorrelation analysis to relate the parameters of the FR defined within our mathematical model to certain observable quantities. This allows us to reconstruct the foregoing parameters and subsequently correct the matched filter. The corrected filter is shown to reduce the distortions of the image

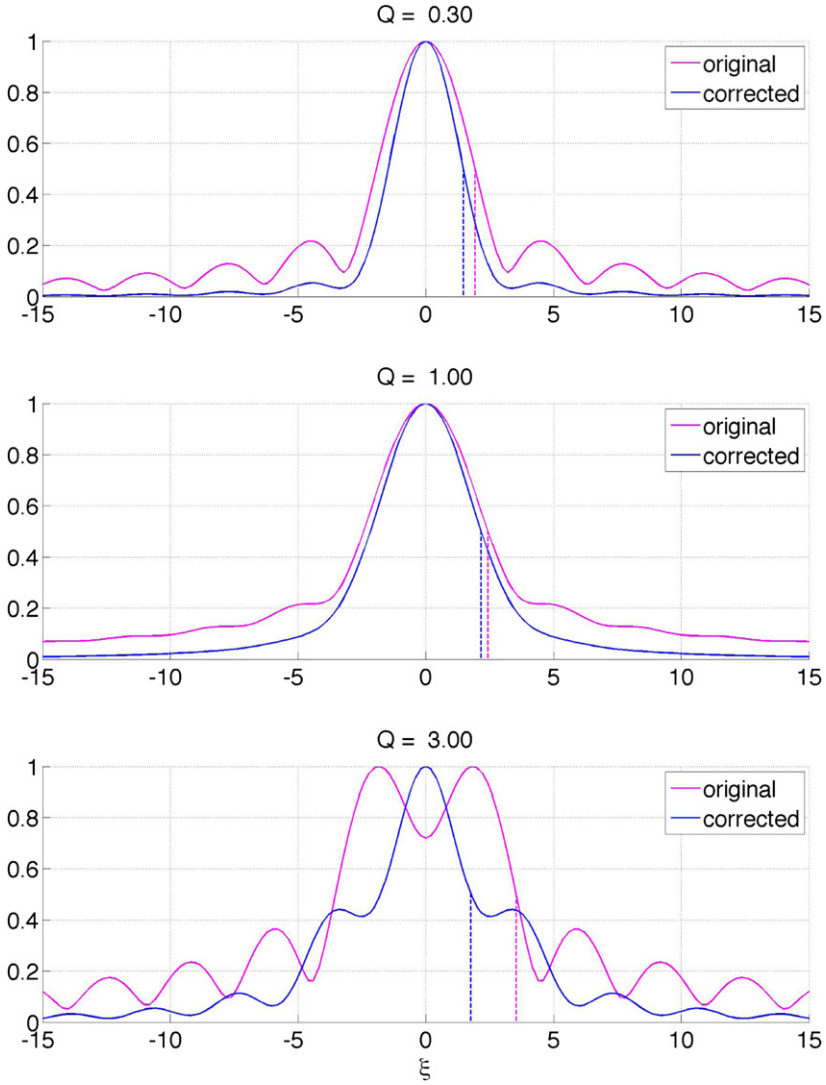

Figure 4. The original and corrected range intensity PSF curves (51) and −3 dB resolution for different values of Q.

due to the FR. It is applied on top of the corrections for the isotropic dispersive propagation, see [1–3].

Our study employs the following simplifying assumptions.

- The scattering model given by (8), (9), see also the remark at the bottom of page 5, does not account for the possible dependence of ground reflectivity on polarization.
- The ACF of target reflectivity is short-range and simplifies to a δ-function, see formula (38).
- No consideration of scattering coherence.
- No explicit treatment of noise or speckle, in particular, when distributed targets are analyzed in section 5.

- Linearization of cosine of the FR angle (22), which may not hold for broadband and/or low frequency radar systems.
- A sinc-type range ambiguity function, see (18); no account of range windowing.

While presenting a certain loss of generality, these assumptions enable a complete quantitative analysis of the effect of frequency-dependent FR on transionospheric SAR imaging. In particular, our approach yields a closed form expression (33) for the GAF modified by the FR. Hence, the analysis of this paper provides a foundation and creates an analytical framework for studying more comprehensive formulations/models in the future.

As indicated in section 5, an issue of interest for the future study is the analysis of sensitivity of the computed parameters of FR to the perturbations in the data. Indeed, while the overall robustness of the proposed algorithm improves as the number of data points increases, higher sensitivity (i.e., poorer conditioning of the roots of equation (46)) implies larger errors and hence requires more data points for reducing those. It will also be of interest to analyze the accuracy of evaluating the image ACF according to (44) (as well as the sensitivity of $g(h)$ to the value of h) because it is precisely the source of the error for the subsequent computation of Q. Then, similarly to how we have looked into the issue of residual distortions when correcting for the effect of the scalar dispersive propagation [3], we will investigate what kind of image distortions one should still anticipate if the parameters of the FR p and q are not known exactly and rather contain some error (due to the inaccuracies in the data).

A very important case is that of a wide range of the FR angle (case (c) on page 10 that is not addressed in this paper, see also figure 3(c)). It will require special attention in the future, because the linearization (22) does not apply. Therefore, this case should be treated differently on both the parameter estimation and filter correction stage. The sub-band processing approach (section 4), if refined and made quantitative, might provide additional estimates of the FR parameters even in this wide-range case.

Some other issues that may be worth attention in the future include:

- Combined analysis of the medium anisotropy and target anisotropy [23].
- A more comprehensive model for electromagnetic wave propagation in the ionospheric plasma that may account, e.g., for Ohmic losses[9].
- Analysis of the FR within the chirp for the fully polarimetric case.
- Incorporation of the improved ground reflectivity models that account for the dependence of the scattered field on the viewing direction and target texture.
- Further investigation of the effect of randomness on SAR images:
  - randomness in the propagation of radar signals through the ionosphere;
  - randomness in the scattering of radar signals off the target.

The propagation of radio waves (radar signals) through the ionosphere acquires stochastic features because the ionospheric plasma is turbulent. Turbulent fluctuations of the electron number density n_e make the Langmuir frequency ω_{pe}, see formula (B.3), a random quantity (more precisely, a random field). In [1–3], we have studied the effect of turbulent fluctuations of n_e on transionospheric SAR imaging in the scalar isotropic framework and under the assumption that the scale of inhomogeneities (fluctuations) is small. In the vector case, the same random quantity ω_{pe} will determine statistics of the FR angle φ_F, because according to (21) φ_F is proportional to $\omega_{pe}^2 \Omega_e \cos\beta$, and neither of the other two factors, Ω_e or $\cos\beta$, formally depends on n_e. The overall considerations, however, may appear more subtle if the

[9] The simplest account of Ohmic losses based on the notion of an effective collision frequency can be found in our previous work [3]. The use of kinetic considerations, see, e.g., [4, chapter II], may be warranted for obtaining a more accurate treatment.

external magnetic field $\boldsymbol{H}_0$ is (partially) frozen into the plasma[10] for the specific conditions of interest. Then, $\boldsymbol{H}_0$ will still fluctuate, and hence the behavior of both Ω_e and $\cos\beta$ in the presence of turbulence will need to be analyzed thoroughly so as to adequately represent the overall statistics of φ_F. Note also that a more comprehensive study that allows for the large scale of turbulent inhomogeneities, yet only for a non-magnetized plasma, can be found in [33].

Acknowledgments

This work was supported by the US Air Force Office of Scientific Research (AFOSR) under agreement FA9550-10-1-0092. We would like to thank the referees of our paper for their helpful comments.

Appendix A. Factorization of the SAR ambiguity function

In this appendix, we analyze the error due to factorization (14) of the GAF (11), (12).

Substituting expressions (12) and (13) into (11), we can write

$$W(\boldsymbol{y},\boldsymbol{z}) = \sum_n \int_\chi \chi_\tau\left(t - t_{\boldsymbol{y}}^n\right) \mathrm{e}^{-\mathrm{i}\alpha(t-t_{\boldsymbol{y}}^n)^2} \mathrm{e}^{-\mathrm{i}\omega_0(t-t_{\boldsymbol{y}}^n)} \chi_\tau\left(t - t_{\boldsymbol{z}}^n\right) \mathrm{e}^{\mathrm{i}\alpha(t-t_{\boldsymbol{z}}^n)^2} \mathrm{e}^{\mathrm{i}\omega_0(t-t_{\boldsymbol{z}}^n)}\, \mathrm{d}t, \tag{A.1}$$

where

$$t_{\boldsymbol{y}}^n \overset{\text{def}}{=} \frac{2R_{\boldsymbol{y}}^n}{c} = \frac{2|\boldsymbol{x}^n - \boldsymbol{y}|}{c} \qquad \text{and} \qquad t_{\boldsymbol{z}}^n \overset{\text{def}}{=} \frac{2R_{\boldsymbol{z}}^n}{c} = \frac{2|\boldsymbol{x}^n - \boldsymbol{z}|}{c}. \tag{A.2}$$

Then, we introduce a new integration variable u and new constants T^n:

$$u = t - \frac{t_{\boldsymbol{z}}^n + t_{\boldsymbol{y}}^n}{2}, \qquad T^n = \frac{t_{\boldsymbol{y}}^n - t_{\boldsymbol{z}}^n}{2} \equiv \frac{R_{\boldsymbol{y}}^n - R_{\boldsymbol{z}}^n}{c}, \tag{A.3}$$

such that

$$t - t_{\boldsymbol{y}}^n = u - T^n \qquad \text{and} \qquad t - t_{\boldsymbol{z}}^n = u + T^n.$$

The travel time between $\boldsymbol{y}$ and $\boldsymbol{z}$ is of the order of $\Delta_R/c \ll \tau$. This is equivalent to $|T^n| \ll \tau$; hence, the two indicator functions χ_τ under the integral in (A.1) overlap on some interval. The center of this interval is $u = 0$ and the endpoints are $u = \tau/2 - |T^n|$ and $u = -\tau/2 + |T^n|$, so that its length is

$$\tau^n = \tau - 2|T^n|. \tag{A.4}$$

The phase of the integrand in (A.1) can be expressed as

$$\begin{aligned} -\alpha(t - t_{\boldsymbol{y}}^n)^2 - \omega_0(t - t_{\boldsymbol{y}}^n) + \alpha(t - t_{\boldsymbol{z}}^n)^2 + \omega_0(t - t_{\boldsymbol{z}}^n) \\ = \alpha[(u + T^n)^2 - (u - T^n)^2] + \omega_0(u + T^n - u + T^n) \\ = \alpha \cdot 4uT^n + 2\omega_0 T^n, \end{aligned}$$

so the integration can be carried out analytically:

$$\begin{aligned} W(\boldsymbol{y},\boldsymbol{z}) &= \sum_n \mathrm{e}^{2\mathrm{i}\omega_0 T^n} \int_{-\tau^n/2}^{\tau^n/2} \mathrm{e}^{4\mathrm{i}\alpha T^n u}\, \mathrm{d}u = \sum_n \mathrm{e}^{2\mathrm{i}\omega_0 T^n} \frac{1}{4\mathrm{i}\alpha T^n} (\mathrm{e}^{\mathrm{i}2\alpha\tau^n T^n} - \mathrm{e}^{-\mathrm{i}2\alpha\tau^n T^n}) \\ &= \sum_n \mathrm{e}^{2\mathrm{i}\omega_0 T^n} \frac{1}{4\mathrm{i}\alpha T^n} 2\mathrm{i}\sin(2\alpha\tau^n T^n) = \sum_n \mathrm{e}^{2\mathrm{i}\omega_0 T^n} \tau^n \operatorname{sinc}(2\alpha\tau^n T^n). \end{aligned} \tag{A.5}$$

[10] In magnetohydrodynamics, saying that the magnetic field is frozen into a plasma emphasizes that the magnetic flux is conserved in the flow of a highly conducting magnetized fluid (Alfvén's theorem), see, e.g., [5, chapter VIII] or [32].

Similarly to (14)–(16), let us now introduce a new function

$$W_{(RA)}(\boldsymbol{y},\boldsymbol{z}) \stackrel{\text{def}}{=} W_R(\boldsymbol{y},\boldsymbol{z}) \cdot W_A(\boldsymbol{y},\boldsymbol{z}), \tag{A.6}$$

where

$$W_A(\boldsymbol{y},\boldsymbol{z}) = \sum_{n=-N/2}^{N/2} \mathrm{e}^{2\mathrm{i}\omega_0(R_y^n - R_z^n)/c} = \sum_n \mathrm{e}^{2\mathrm{i}\omega_0 T^n} \tag{A.7}$$

and

$$W_R(\boldsymbol{y},\boldsymbol{z}) = \int_\chi \overline{A\big(u_y^0\big)} A\big(u_z^0\big)\,\mathrm{d}t = \tau^0\,\mathrm{sinc}(2\alpha\tau^0 T^0). \tag{A.8}$$

In formula (A.8), τ^0 and T^0 denote τ^n and T^n, respectively, for $n = 0$. Our goal is to determine how accurately this new function $W_{(RA)}(\boldsymbol{y},\boldsymbol{z})$ of (A.6)–(A.8) will approximate the GAF $W(\boldsymbol{y},\boldsymbol{z})$ of (A.1) or, equivalently, (A.5). To determine the accuracy of approximation, we will estimate the error

$$W - W_{(RA)} = \sum_n \mathrm{e}^{2\mathrm{i}\omega_0 T^n}[\tau^n\,\mathrm{sinc}(2\alpha\tau^n T^n) - \tau^0\,\mathrm{sinc}(2\alpha\tau^0 T^0)]. \tag{A.9}$$

The Pythagorean theorem for R_y^n and R_z^n (see figure 1) yields:

$$\begin{aligned}(R_z^n)^2 &= |\boldsymbol{z} - \boldsymbol{x}^n|^2 = H^2 + L^2 + (x_1^n)^2 = R^2 + (x_1^n)^2\\ (R_y^n)^2 &= |\boldsymbol{y} - \boldsymbol{x}^n|^2 = H^2 + (L+l)^2 + (x_1^n - y_1)^2\\ &= R^2 + 2Ll + l^2 + (x_1^n - y_1)^2,\end{aligned} \tag{A.10}$$

where

$$L = z_2 = R\sin\theta \quad \text{and} \quad l = y_2 - z_2.$$

For the physical distances involved, we take

$$R \sim L \sim 10^6 m, \quad |x_1^n| \lesssim 10^4 m, \quad \text{and} \quad |y_1| \sim |l| \lesssim 10^2 m.$$

Then, using the Taylor formula $(1+\xi)^{1/2} \approx 1 + \frac{1}{2}\xi$ for $|\xi| \ll 1$ we get

$$\frac{R_z^n}{R} \approx 1 + \frac{(x_1^n)^2}{2R^2} \quad \text{and} \quad \frac{R_y^n}{R} \approx 1 + \frac{1}{2}\frac{l^2 + 2lL + (x_1^n)^2 - 2x_1^n y_1 + y_1^2}{R^2},$$

which, after keeping only the leading order term that does not depend on n and the leading term that depends on n, yields:

$$\frac{R_y^n - R_z^n}{R} \approx \frac{L}{R}\frac{l}{R} - \frac{x_1^n y_1}{R^2}. \tag{A.11}$$

Consequently, we have

$$T^n \approx \frac{1}{c}\left(l\sin\theta - y_1\frac{x_1^n}{R}\right) \stackrel{\text{def}}{=} T^0 - \mathcal{T}^n, \tag{A.12}$$

where, taking into account that $x_1^n = n\Delta x_1 = nL_{\mathrm{SA}}/N$, we have introduced

$$T^0 = \frac{l\sin\theta}{c}, \quad \mathcal{T}^1 = \frac{y_1\Delta x_1}{cR} = \frac{y_1 L_{\mathrm{SA}}}{NcR}, \quad \text{and} \quad \mathcal{T}^n = \frac{y_1 x_1^n}{cR} = n\mathcal{T}^1. \tag{A.13}$$

As $|T^0| \ll \tau$ and $|\mathcal{T}^n| \ll \tau$, we can write using the first-order Taylor formula:

$$\mathrm{sinc}(2\alpha\tau^n T^n) \approx \mathrm{sinc}(2\alpha\tau^0 T^0) - 2\alpha\tau^0\mathcal{T}^n\,\mathrm{sinc}'(2\alpha\tau^0 T^0), \tag{A.14}$$

so that the expression in the square brackets in (A.9) evaluates to

$$\tau^n\,\mathrm{sinc}(2\alpha\tau^n T^n) - \tau^0\,\mathrm{sinc}(2\alpha\tau^0 T^0) \approx \mathcal{T}^n S = Sn\mathcal{T}^1,$$

where

$$S = \operatorname{sinc}(2\alpha\tau^0 T^0) - 2\alpha(\tau^0)^2 \operatorname{sinc}'(2\alpha\tau^0 T^0). \tag{A.15}$$

Hence, formula (A.9) transforms into

$$W - W_{(RA)} \approx \mathrm{e}^{\mathrm{i}\Phi_0} S \sum_n \mathrm{e}^{-2\mathrm{i}\omega_0 \mathcal{T}^n} \mathcal{T}^n = S\mathcal{T}^1 \mathrm{e}^{\mathrm{i}\Phi_0} \sum_{n=-N/2}^{N/2} n\,\mathrm{e}^{\mathrm{i}n\varphi}, \tag{A.16}$$

where

$$\Phi_0 = 2\frac{\omega_0 l}{c}\sin\theta \quad \text{and} \quad \varphi = -2\omega_0\mathcal{T}^1 = -2\frac{\omega_0 L_{\mathrm{SA}}}{NRc}y_1.$$

Note that Φ_0 defined above is not quite identical to the one in formula (17), but the discrepancy is small, on the order of those terms neglected when deriving (A.11).

To perform the summation in (A.16), we first use the standard summation of a geometric sequence:

$$\sum_{n=-N/2}^{N/2} \mathrm{e}^{\mathrm{i}n\varphi} = \frac{\sin(\varphi(N+1)/2)}{\sin(\varphi/2)} \approx N \operatorname{sinc}\frac{N\varphi}{2}, \tag{A.17}$$

where the last approximate equality holds provided that $|\varphi| \ll 1$, i.e., $\pi y_1/(\Delta_A N) \ll 1$. Then, differentiating both sides of (A.17) w.r.t. φ we get

$$\sum_{n=-N/2}^{N/2} n\mathrm{e}^{\mathrm{i}n\varphi} = \frac{1}{\mathrm{i}}\frac{\partial}{\partial\varphi}\sum_{n=-N/2}^{N/2} \mathrm{e}^{\mathrm{i}n\varphi} \approx \frac{1}{\mathrm{i}}\frac{\partial}{\partial\varphi}\left(N\operatorname{sinc}\frac{N\varphi}{2}\right) = \frac{N^2}{2\mathrm{i}}\operatorname{sinc}'\frac{N\varphi}{2}.$$

Therefore, the expression in (A.16) evaluates to

$$\begin{aligned} W - W_{(RA)} &\approx S\mathcal{T}^1\frac{N^2}{2\mathrm{i}}\mathrm{e}^{\mathrm{i}\Phi_0}\operatorname{sinc}'\frac{N\varphi}{2} = \frac{\mathrm{i}\mathrm{e}^{\mathrm{i}\Phi_0}}{2\omega_0}NSY_1\operatorname{sinc}' Y_1 \\ &= \frac{\mathrm{i}\mathrm{e}^{\mathrm{i}\Phi_0}}{2\omega_0}N(\operatorname{sinc}(2\alpha\tau^0 T^0) - 2\alpha(\tau^0)^2\operatorname{sinc}'(2\alpha\tau^0 T^0))Y_1\operatorname{sinc}' Y_1, \end{aligned} \tag{A.18}$$

where $Y_1 = -N\varphi/2 = \pi y_1/\Delta_A$. Formula (A.18) provides an expression for the factorization error (A.9) that we will now estimate. Let us first assume that

$$|Y_1| \lesssim 1, \quad |\operatorname{sinc}' Y_1| \lesssim 1, \quad \text{and} \quad |\operatorname{sinc}'(2\alpha\tau^0 T^0)| \lesssim 1,$$

which is reasonable to expect. Then, let us notice that as $2\alpha(\tau^0)^2 \approx B\tau \gg 1$, the second term on the right-hand side of formula (A.15) is much greater than the first one (except for very small T^0, i.e., when $\boldsymbol{y}$ and $\boldsymbol{z}$ are nearly at the same range). Hence, we can keep only the second (dominant) term for S and obtain using (A.7), (A.8), and (A.18):

$$\frac{|\max(W - W_{(RA)})|}{|\max W_{(RA)}|} \sim \frac{1}{N\tau}\frac{N}{2\omega_0}2\alpha\tau^2 = \frac{1}{2}\frac{B}{\omega_0}. \tag{A.19}$$

Formula (A.19) provides an estimate for the relative error due to the factorization (A.6)–(A.8) or, equivalently, (14)–(16). This error may be on the order of a few percent depending on the value of the relative bandwidth $\frac{B}{\omega_0}$. It is interesting to note that according to (A.18), the dominant term of this error vanishes if either $y_2 = z_2$ or $y_1 = 0$ (the latter is equivalent to $y_1 = z_1$). The key to understanding this effect is the expression for T^n in (A.12)–(A.13). Physically, T^n is the difference between the pulse two-way travel time for the pairs $(\boldsymbol{x}^n, \boldsymbol{y})$ and $(\boldsymbol{x}^n, \boldsymbol{z})$. As a function of the satellite position n, T^n has a constant part T^0 and a part $\mathcal{T}^n$ which is linear in n. It is the variation of the range PSF $\operatorname{sinc}(2\alpha\tau^n T^n)$ with n in formula (A.5) that is responsible for the leading term of the factorization error. If $y_2 = z_2$, then the constant part of T^n vanishes and so does the PSF tangent slope given by $\operatorname{sinc}'(2\alpha\tau^0 T^0)$.

Hence, the leading term of the variation of the PSF magnitude disappears. If, however, $y_1 = 0$ (or $y_1 = z_1$), then it is the leading term of the variation of T^n with n that vanishes [$\mathcal{T}^n \equiv 0$, see (A.13)], and so does the leading term of the variation of $\mathrm{sinc}(2\alpha\tau^n T^n)$ regardless of the value of $2\alpha\tau^0 T^0$. Only in the general 'diagonal' configuration $y_1 \neq z_1$, $y_2 \neq z_2$ the coupling between the range and azimuthal terms is significant, yielding the error (A.18).

Appendix B. Faraday rotation for a chirped signal

Plane time-harmonic waves

$$(\boldsymbol{E}, \boldsymbol{H}) \sim \mathrm{e}^{\mathrm{i}(\omega t - \boldsymbol{k}\boldsymbol{r})}$$

in a cold magnetized plasma are governed by the following equation (see, e.g., [4, 34]):

$$\Lambda_{ij} E_j \equiv \left[\frac{k^2 c^2}{\omega^2} \left(\frac{k_i k_j}{k^2} - \delta_{ij} \right) + \varepsilon_{ij} \right] E_j = 0. \tag{B.1}$$

Let the constant external magnetic field $\boldsymbol{H}_0$ be aligned with the z-axis[11]. Then, the dielectric tensor $\varepsilon = \{\varepsilon_{ij}\}$ in (B.1) has the form

$$\varepsilon = \begin{pmatrix} \varepsilon_\perp & -\mathrm{i}g & 0 \\ \mathrm{i}g & \varepsilon_\perp & 0 \\ 0 & 0 & \varepsilon_\parallel \end{pmatrix},$$

where

$$\begin{aligned} \varepsilon_\parallel &= 1 - \frac{\omega_{\mathrm{pe}}^2}{\omega^2} - \frac{\omega_{\mathrm{pi}}^2}{\omega^2}, \\ \varepsilon_\perp &= 1 - \frac{\omega_{\mathrm{pe}}^2}{\omega^2 - \Omega_{\mathrm{e}}^2} - \frac{\omega_{\mathrm{pi}}^2}{\omega^2 - \Omega_{\mathrm{i}}^2}, \\ g &= \frac{\omega_{\mathrm{pe}}^2 \Omega_{\mathrm{e}}}{\omega(\omega^2 - \Omega_{\mathrm{e}}^2)} - \frac{\omega_{\mathrm{pi}}^2 \Omega_{\mathrm{i}}}{\omega(\omega^2 - \Omega_{\mathrm{i}}^2)}. \end{aligned} \tag{B.2}$$

In formulae (B.2), ω_{pe} and ω_{pi} denote the electron and ion Langmuir frequencies, while Ω_{e} and Ω_{i} denote the electron and ion Larmor frequencies, respectively:

$$\omega_{\mathrm{pe,pi}} = \left(\frac{4\pi n_{\mathrm{e,i}} e^2}{m_{\mathrm{e,i}}} \right)^{1/2} \text{ and } \Omega_{\mathrm{e,i}} = \frac{e|\boldsymbol{H}_0|}{m_{\mathrm{e,i}} c}. \tag{B.3}$$

In formulae (B.3), $n_{\mathrm{e,i}}$ is the particle number density, and $m_{\mathrm{e,i}}$ is the particle mass. As ions are much heavier than electrons: $m_{\mathrm{i}} \gg m_{\mathrm{e}}$, we can write according to (B.3):

$$\omega_{\mathrm{pe}} \gg \omega_{\mathrm{pi}} \quad \text{and} \quad \Omega_{\mathrm{e}} \gg \Omega_{\mathrm{i}}. \tag{B.4}$$

We also note that for the typical values of $n_{\mathrm{e,i}}$ and $|\boldsymbol{H}_0|$ the following relations hold:

$$\omega_{\mathrm{pe}} \gg \Omega_{\mathrm{e}} \quad \text{and} \quad \omega_{\mathrm{pi}} \gg \Omega_{\mathrm{i}}. \tag{B.5}$$

Finally, for the interrogating frequency we are assuming that

$$\omega \gg \omega_{\mathrm{pe}}. \tag{B.6}$$

Relations (B.4)–(B.6) allow us to disregard the contribution of ions to dielectric properties of the ionospheric plasma, because the terms due to ions on the right-hand side of equalities (B.2) appear much smaller than the respective terms due to electrons.

[11] In this appendix, we use the *xyz*-notation for the coordinates.

The dispersion relation for the waves governed by equation (B.1) is

$$\det \Lambda = 0, \tag{B.7}$$

and the corresponding non-trivial solutions $\boldsymbol{E}$ are called the polarization vectors. For simplicity, we first consider the case of a parallel propagation:

$$|\boldsymbol{k}| = |k_z|, \quad k_x = k_y = 0. \tag{B.8}$$

If there is no magnetic field, then $\Omega_{\mathrm{e,i}} = 0$, the matrices ε and Λ are diagonal, and there are two types of polarization: longitudinal, $\boldsymbol{E} = (0, 0, E_z)$, and transverse, $\boldsymbol{E} = (E_x, E_y, 0)$. In doing so, one of the transverse polarization vectors can be chosen with $E_x = 0$ and the other with $E_y = 0$, which corresponds to two linear polarizations. When $\Omega_{\mathrm{e}} \neq 0$, (B.7) yields the following dispersion relation for transverse waves ($E_z = 0$):

$$\frac{(k^{\pm})^2 c^2}{\omega^2} = 1 - \frac{\omega_{\mathrm{pe}}^2}{\omega^2} \pm \frac{\omega_{\mathrm{pe}}^2 \Omega_{\mathrm{e}}}{\omega^3} = 1 - f_1 \pm f_2, \tag{B.9}$$

where we have introduced the notations

$$f_1 \equiv f_1(\omega) = \frac{\omega_{\mathrm{pe}}^2}{\omega^2}, \quad f_2 \equiv f_2(\omega) = \frac{\omega_{\mathrm{pe}}^2 \Omega_{\mathrm{e}}}{\omega^3}, \quad \text{and} \quad 1 \gg f_1 \gg f_2. \tag{B.10}$$

Solutions to equation (B.9) correspond to two polarization vectors:

$$\begin{pmatrix} E_x \\ E_y \end{pmatrix} \sim \begin{pmatrix} 1 \\ \pm i \end{pmatrix}, \tag{B.11}$$

that represent two circular polarizations with opposite direction of rotation. The phase and group velocities for these two circularly polarized waves are given by

$$v_{\mathrm{ph}}^{\pm} \stackrel{\mathrm{def}}{=} \frac{\omega}{k^{\pm}} = c(1 - f_1 \pm f_2)^{-1/2}, \tag{B.12a}$$

$$v_{\mathrm{gr}}^{\pm} \stackrel{\mathrm{def}}{=} \left(\frac{\mathrm{d}\omega}{\mathrm{d}k}\right)^{\pm} = \left(\frac{1}{v_{\mathrm{ph}}^{\pm}} + \frac{\omega^2}{2k^{\pm}c^2}(-f_1' \pm f_2')\right)^{-1}. \tag{B.12b}$$

Formulae (B.12) along with (B.5), (B.6) and (B.10) indicate that the terms due to the magnetic field $\boldsymbol{H}_0$ (i.e., proportional to f_2) have a very small effect on v_{gr} and v_{ph}. The only situation where this effect can be seen is when the terms of order 1 and f_1 cancel, which happens when one evaluates the difference between the propagation speeds for two circular polarizations: $(v_{\mathrm{gr}}^{+} - v_{\mathrm{gr}}^{-})$ or $(v_{\mathrm{ph}}^{+} - v_{\mathrm{ph}}^{-})$. It is the phase speed difference that is responsible for the FR.

The expression for the chirp (4)–(5) traveling through an isotropic ionosphere (no external magnetic field and no FR) has been obtained in [2, Appendix A] by Fourier transforming the initial pulse in time, propagating each harmonic in space with the corresponding phase velocity, and finally making the inverse Fourier transform:

$$\begin{aligned} \varphi(t, r) &= \frac{1}{4\pi r} \mathrm{e}^{\mathrm{i}\omega_0(t - r/v_{\mathrm{ph}_0})} \chi_{\tau'}(t - r/v_{\mathrm{gr}_0}) \, \mathrm{e}^{\mathrm{i}\alpha'(t - r/v_{\mathrm{gr}_0})^2} \\ &\stackrel{\mathrm{def}}{=} \frac{1}{4\pi r} A'(t - r/v_{\mathrm{gr}_0}) \, \mathrm{e}^{\mathrm{i}\omega_0(t - r/v_{\mathrm{ph}_0})}, \end{aligned} \tag{B.13}$$

where

$$\tau' = \tau - \delta\tau = \tau - \frac{r}{c}\frac{\omega_{\mathrm{pe}}^2}{\omega_0^2}\frac{B}{\omega_0} \quad \text{and} \quad \alpha' = \alpha + \delta\alpha = \frac{B}{2\tau}\left(1 + \frac{\delta\tau}{\tau}\right) \tag{B.14}$$

are the modified chirp parameters that account for the temporal dispersion. Hereafter, v_{ph_0}, v_{gr_0}, and k_0 refer to the phase and group velocities and the wavenumber for the isotropic

plasma, i.e., calculated according to (B.9) and (B.12) at $\omega = \omega_0$ with $f_2 = 0$. Formulae (B.13)–(B.14) describe a modified linear upchirp (with a shorter duration and higher rate). These formulae, however, were obtained in [2, 3] by linearizing the dispersion relation around ω_0 and excluding the frequencies outside the chirp bandwidth (6) from the propagation analysis (or, equivalently, by disregarding the precursors). Without these simplifications, the received signal will not necessarily be a chirp.

For the case of a magnetized plasma, formula (B.13) can be extended to the circularly polarized waves. Considering the form of the polarization vectors in (B.11), the expressions for the propagating circular harmonics are

$$\begin{pmatrix} E_x \\ E_y \end{pmatrix}(t, r) = \begin{pmatrix} 1 \\ \pm \mathrm{i} \end{pmatrix} \frac{1}{4\pi r} A'(t - r/v_{\mathrm{gr}}^{\pm})\, \mathrm{e}^{\mathrm{i}\omega_0 (t - r/v_{\mathrm{ph}}^{\pm})}$$

and the total propagating field is a linear combination of those

$$\begin{aligned} \begin{pmatrix} E_x \\ E_y \end{pmatrix}(t, r) &\propto \frac{1}{4\pi r} \sum_{\pm} \begin{pmatrix} 1 \\ \pm \mathrm{i} \end{pmatrix} C_{\pm} A'(t - r/v_{\mathrm{gr}}^{\pm})\, \mathrm{e}^{\mathrm{i}\omega_0 (t - r/v_{\mathrm{ph}}^{\pm})} \\ &= \frac{1}{4\pi r} \sum_{\pm} \begin{pmatrix} 1 \\ \pm \mathrm{i} \end{pmatrix} C_{\pm} \chi_{\tau'}(t - r/v_{\mathrm{gr}_0})\, \mathrm{e}^{\mathrm{i}\alpha'(t - r/v_{\mathrm{gr}}^{\pm})^2}\, \mathrm{e}^{\mathrm{i}\omega_0 (t - r/v_{\mathrm{ph}}^{\pm})}, \end{aligned} \tag{B.15}$$

where $C_{\pm}$ are the amplitudes. To make the emitted field ($r = 0$) linearly polarized in the xz-plane, we set $C_+ = C_- = 1$. Per our earlier discussion, in the argument of $\chi_{\tau'}$ on the second line of (B.15) we leave out the effect of polarization on the chirp boundaries.

Introduce the 'chirp time' variable

$$u \stackrel{\mathrm{def}}{=} t - \frac{r}{v_{\mathrm{gr}_0}} \quad \text{so that} \quad -\frac{\tau'}{2} < u < \frac{\tau'}{2}.$$

For the retarded group travel time in (B.15), we have:

$$\begin{aligned} t_{\mathrm{gr}}^{\pm} \stackrel{\mathrm{def}}{=} t - \frac{r}{v_{\mathrm{gr}}^{\pm}} &= u + r\left(\frac{1}{v_{\mathrm{gr}_0}} - \frac{1}{v_{\mathrm{gr}}^{\pm}}\right) = u + r\left(\frac{k_0}{\omega_0} - \frac{\omega_0^2}{2k_0c^2} f_1' - \frac{k^{\pm}}{\omega_0} + \frac{\omega_0^2}{2k^{\pm}c^2}(f_1' \mp f_2')\right) \\ &= u + r\left(\frac{k_0 - k^{\pm}}{\omega_0} + \frac{\omega_0^2 f_1'}{2c^2}\left(\frac{1}{k^{\pm}} - \frac{1}{k_0}\right) \mp \frac{\omega_0^2}{2k^{\pm}c^2} f_2'\right) \\ &= u + r\frac{k_0 - k^{\pm}}{\omega_0}\left(1 + \frac{\omega_0^3}{2c^2 k_0 k^{\pm}} f_1'\right) \mp r\frac{\omega_0^2}{2k^{\pm}c^2} f_2' \\ &\approx u + r\frac{k_0 - k^{\pm}}{\omega_0} \mp r\frac{\omega_0^2}{2k_0^2c^2} f_2' \approx u \mp \frac{r}{2c} f_2 \mp r\frac{\omega_0^2}{2k_0^2c^2} f_2'. \end{aligned}$$

From (B.10), we obtain $f_2'(\omega) = -3\omega_{\mathrm{pe}}^2 \Omega_{\mathrm{e}}/\omega^4$, and therefore

$$t_{\mathrm{gr}}^{\pm} \approx u \mp \frac{r}{2c} \frac{\omega_{\mathrm{pe}}^2 \Omega_{\mathrm{e}}}{\omega_0^3}\left(1 - 3\frac{\omega_0}{k_0 c}\right) \approx u \pm \frac{r}{c} f_2. \tag{B.16a}$$

For the retarded phase travel time, we can write:

$$\begin{aligned} t_{\mathrm{ph}}^{\pm} \stackrel{\mathrm{def}}{=} t - \frac{r}{v_{\mathrm{ph}}^{\pm}} &= u + r\left(\frac{1}{v_{\mathrm{gr}_0}} - \frac{1}{v_{\mathrm{ph}}^{\pm}}\right) = u + r\left(\frac{1}{v_{\mathrm{gr}_0}} - \frac{1}{v_{\mathrm{ph}_0}}\right) + r\left(\frac{1}{v_{\mathrm{ph}_0}} - \frac{1}{v_{\mathrm{ph}}^{\pm}}\right) \\ &\approx u + r s_0 \mp \frac{r}{2c} f_2, \end{aligned} \tag{B.16b}$$

where the dispersive term

$$s_0 \stackrel{\mathrm{def}}{=} \frac{1}{v_{\mathrm{gr}_0}} - \frac{1}{v_{\mathrm{ph}_0}}$$

is the same for both polarizations. Substituting (B.16) into (B.15), we get

$$\begin{aligned}\begin{pmatrix}E_x\\E_y\end{pmatrix}(t,r) &\propto \chi_{\tau'}(u)\sum_{\pm}\begin{pmatrix}1\\\pm i\end{pmatrix}\mathrm{e}^{\mathrm{i}\alpha'(u^2\pm 2u\frac{r}{c}f_2)}\mathrm{e}^{\mathrm{i}\omega_0(u+rs_0\mp\frac{r}{2c}f_2)}\\ &= \chi_{\tau'}(u)\sum_{\pm}\begin{pmatrix}1\\\pm i\end{pmatrix}\mathrm{e}^{\mathrm{i}\omega_0(u+rs_0)+\mathrm{i}\alpha' u^2}\,\mathrm{e}^{\mp\mathrm{i}\varphi_F},\end{aligned}\tag{B.17}$$

where

$$\varphi_F = \frac{\omega_0 r}{2c}f_2 - 2\alpha' u\frac{r}{c}f_2 = \frac{r}{2c}\omega_{\mathrm{pe}}^2\Omega_{\mathrm{e}}\left[\frac{1}{\omega_0^2} + 2\alpha' u\cdot\left(\frac{\mathrm{d}}{\mathrm{d}\omega}\frac{1}{\omega^2}\right)\Big|_{\omega=\omega_0}\right].\tag{B.18}$$

Per our definitions of u and s_0, we see that the phase in the first exponent of (B.17) is equivalent to the one in the isotropic dispersive propagator (B.13):

$$\begin{aligned}\omega_0(u+rs_0)+\alpha' u^2 &= \omega_0\left[t-\frac{r}{v_{\mathrm{gr}_0}}+r\left(\frac{1}{v_{\mathrm{gr}_0}}-\frac{1}{v_{\mathrm{ph}_0}}\right)\right]+\alpha'\left(t-\frac{r}{v_{\mathrm{gr}_0}}\right)^2\\ &= \omega_0\left(t-\frac{r}{v_{\mathrm{ph}_0}}\right)+\alpha'\left(t-\frac{r}{v_{\mathrm{gr}_0}}\right)^2.\end{aligned}$$

The quantity φ_F in the last exponent of (B.17) is the FR angle which is equal to one half of the difference between the phases of circularly polarized harmonics:

$$\begin{pmatrix}E_x\\E_y\end{pmatrix}(t,r)\sim\begin{pmatrix}\cos\varphi_F\\\sin\varphi_F\end{pmatrix}A'(t-r/v_{\mathrm{gr}_0})\,\mathrm{e}^{\mathrm{i}\omega_0(t-r/v_{\mathrm{ph}_0})}.\tag{B.19}$$

The expression in the square brackets in (B.18) may be interpreted as the function $f(\omega)=\frac{1}{\omega^2}$ evaluated at the instantaneous frequency $\omega=\omega_0+2\alpha' u$, cf formula (6), by means of a first-order Taylor formula. Except for the small difference between α' and α, the expression for the FR as a function of the instantaneous frequency in (B.18) coincides with the intuitive formula (21) for $r=2R$ and $\beta=0$.

For oblique propagation, i.e., when $|k_z|<|\boldsymbol{k}|$ and $\beta\neq 0$, a careful analysis shows (see [4]) that except in a very narrow range of nearly transverse propagation angles β, viz $|\cos\beta|\lesssim\frac{\Omega_{\mathrm{e}}}{\omega_0}$, the results obtained for the parallel case (B.8) extend to the oblique case once Ω_{e} is replaced by $\Omega_{\mathrm{e}}\cos\beta$, which, again, transforms (B.18) into (21). Thus,

$$\varphi_F(\omega)=\frac{r}{2c}\frac{\omega_{\mathrm{pe}}^2\Omega_{\mathrm{e}}\cos\beta}{\omega^2}\tag{B.20}$$

is an expression for the FR angle of different parts of a linear chirp parameterized by the instantaneous frequency ω.

Appendix C. Faraday rotation and dispersion-compensated matched filter

In this appendix, we show that the effect of dispersive propagation on SAR imaging analyzed in [1–3] can be separated from that of the FR. Given the form (B.13)–(B.14) of the radar pulse propagating in an isotropic plasma, the matched filter focused at the reference point $\boldsymbol{y}$ and corrected for dispersion (but not the FR) should be taken as

$$\begin{aligned}&\overline{A_{\tau'}(t-2R_{\boldsymbol{y}}/v_{\mathrm{gr}_0})\,\mathrm{e}^{\mathrm{i}\omega_0(t-2R_{\boldsymbol{y}}/v_{\mathrm{ph}_0})}}\\ &\qquad=\chi_{\tau'}(t-2R_{\boldsymbol{y}}/v_{\mathrm{gr}_0})\,\mathrm{e}^{-\mathrm{i}\alpha'(t-2R_{\boldsymbol{y}}/v_{\mathrm{gr}_0})^2}\,\mathrm{e}^{-\mathrm{i}\omega_0(t-2R_{\boldsymbol{y}}/v_{\mathrm{ph}_0})},\end{aligned}\tag{C.1}$$

where the travel distance $2R_y$ accounts for the round-trip. Let us also introduce the following 'dispersive' quantities that replace those of (A.2)–(A.4):

$$t_y^{n\prime} = \frac{2R_y^n}{v_{\mathrm{gr}_0}}, \quad t_z^{n\prime} = \frac{2R_z^n}{v_{\mathrm{gr}_0}}, \quad u' = t - \frac{t_z^{n\prime} + t_y^{n\prime}}{2},$$
$$T^{n\prime} = \frac{t_y^{n\prime} - t_z^{n\prime}}{2}, \quad \tau^{n\prime} = \tau - 2|T^{n\prime}|, \quad \omega_0' = \frac{v_{\mathrm{gr}_0}}{v_{\mathrm{ph}_0}}\omega_0. \tag{C.2}$$

Applying the filter (C.1) to the dispersive propagator (B.13)–(B.14), and using the primed variables of (C.2) and (B.14) instead of their non-primed counterparts, we will arrive at a primed equivalent of (A.1). Then, performing the integration we have:

$$W'(\boldsymbol{y}, \boldsymbol{z}) = \sum_n \mathrm{e}^{2\mathrm{i}\omega_0' T^{n\prime}} \sum_n \int_{-\tau^{n\prime}/2}^{\tau^{n\prime}/2} \mathrm{e}^{4\mathrm{i}\alpha' T^{n\prime} u'} \,\mathrm{d}u'. \tag{C.3}$$

Expression (C.3) is the GAF obtained with a dispersion corrected matched filter in the isotropic dispersive case. The functional dependence on all the parameters in formula (C.3) is exactly the same as that in its non-dispersive counterpart (A.5). The only difference is that all the parameters in formula (C.3) are primed, see (C.2).

Hence, in the case of a dispersive isotropic medium and corrected matched filter, one can drop the primes and use the non-dispersive expressions for the GAF, see (11)–(12). Factorization (14)–(16) can also be used, because the reasoning of the rest of appendix A applies with no changes. We emphasize that in doing so the dispersion is not disregarded. It is rather the opposite, we restore the non-dispersive performance in the dispersive case by correcting the filter accordingly. There will only be negligible discrepancies in final results (e.g., the resolution) between the dispersive and non-dispersive case that are due to different numerical values of the primed and non-primed parameters in (B.14), (C.2) and in (4), (5), (A.2), (A.3).

Let us now see how the filter corrected for dispersion acts on a linearly polarized chirp that propagates in a medium that is both dispersive and gyrotropic, see appendix B. From (B.19), we get the following relation between the actual signal $\psi_F(t, \boldsymbol{x})$ and the hypothetical signal $\psi(t, \boldsymbol{x})$ obtained if there were no FR:

$$\psi_F(t, \boldsymbol{x}) = \psi(t, \boldsymbol{x}) \cos\varphi_F. \tag{C.4}$$

If the reflected field in (C.4) is due to a scatterer at $\boldsymbol{z}$, then the application of the filter (C.1) yields the following expression instead of (A.1):

$$W_F = \sum_n \int_\chi \overline{A_{\tau'}(t - t_y^{n\prime})\,\mathrm{e}^{\mathrm{i}\omega_0'(t' - t_y^{n\prime})}} A_{\tau'}(t - t_z^{n\prime})\,\mathrm{e}^{\mathrm{i}\omega_0'(t' - t_z^{n\prime})} \cos\varphi_F(t - t_z^{n\prime})\,\mathrm{d}t, \tag{C.5}$$

where $t' = t v_{\mathrm{ph}_0}/v_{\mathrm{gr}_0}$ and φ_F is given by (B.18) with $r = 2R_z$ and $u = t - t_z^{n\prime}$. The terms $\omega_0' t'$ in the exponents in (C.5) cancel out. Apart from those, the difference between (C.5) and (A.1) is two-fold: equation (C.5) involves the primed constants of (B.14), (C.2) and the amplitude factor $\cos\varphi_F$ that varies over the chirp. As we have shown, all the functional dependences in the GAF are the same in the primed case as in the non-primed case, with only minute additional distortions. Therefore, we can drop the primes in (C.5) as well, which yields equation (27), and focus only on the effect of the FR on imaging, which manifests itself through the magnitude variation $\propto \cos\varphi_F$.

Remark. As shown in appendix B, the physical origin of the FR is dispersion, see equation (B.9). Hence, thinking that one can ignore the isotropic part of dispersion f_1 and consider only the role of its anisotropic part f_2 may be confusing. Moreover, as $f_1 \gg f_2$, see (B.10), the effect of the isotropic part of dispersion on the *signal* is greater than that due to the magnetic

field. It is actually the use of the modified chirp parameters (B.13)–(B.14) in the matched filter in (24) and (28) that allows one to compensate for the distortions due to f_1 and thus isolate the effect of anisotropy on the *GAF*.

Appendix D. Factorization of the SAR ambiguity function in the presence of Faraday rotation

Our goal here is to perform the analysis similar to that in appendix A, but taking into account the FR, i.e., evaluate the error due to the factorization (29) of the GAF (27)–(28). In (C.5), we drop the primes and linearize $\cos\varphi_F(u)$ around $u=0$ (cf (22)):

$$\cos\varphi_F(u_z^n) \approx p + \frac{2q}{\tau}u_z^n, \tag{D.1}$$

where p and q are defined in (23). This yields the GAF (27)–(28), which we write as

$$W_F(\boldsymbol{y},\boldsymbol{z}) = pW(\boldsymbol{y},\boldsymbol{z}) + q\frac{2}{\tau}W_q(\boldsymbol{y},\boldsymbol{z}),$$

where $W(\boldsymbol{y},\boldsymbol{z})$ is given by (A.1), and

$$W_q(\boldsymbol{y},\boldsymbol{z}) = \sum_n \int_\chi \chi_\tau\big(t-t_y^n\big)\,\mathrm{e}^{-\mathrm{i}\alpha(t-t_y^n)^2}\,\mathrm{e}^{-\mathrm{i}\omega_0(t-t_y^n)}\chi_\tau\big(t-t_z^n\big)\,\mathrm{e}^{\mathrm{i}\alpha(t-t_z^n)^2}\,\mathrm{e}^{\mathrm{i}\omega_0(t-t_z^n)}\big(t-t_z^n\big)\,\mathrm{d}t. \tag{D.2}$$

It is the last factor $(t-t_z^n)$ under the integral that distinguishes W_q of (D.2) from W of (A.1). Using the substitutions from (A.2) and (A.3), we transform (D.2) into (cf (A.5))

$$W_q = \sum_n \mathrm{e}^{2\mathrm{i}\omega_0 T^n}\int_{-\tau^n/2}^{\tau^n/2}\mathrm{e}^{4\mathrm{i}\alpha T^n u}(u+T^n)\,\mathrm{d}u = W_{q1}+W_{q2}, \tag{D.3}$$

where the terms W_{q1} and W_{q2} originate from u and T^n in the round brackets, respectively.

The term W_{q1} can be evaluated as follows:

$$\begin{aligned} W_{q1} &= \sum_n \mathrm{e}^{2\mathrm{i}\omega_0 T^n}\int_{-\tau^n/2}^{\tau^n/2}\mathrm{e}^{4\mathrm{i}\alpha T^n u}u\,\mathrm{d}u = \sum_n \mathrm{e}^{2\mathrm{i}\omega_0 T^n}\frac{1}{4\mathrm{i}T^n}\frac{\partial}{\partial\alpha}\int_{-\tau^n/2}^{\tau^n/2}\mathrm{e}^{4\mathrm{i}\alpha T^n u}\,\mathrm{d}u \\ &= \sum_n \mathrm{e}^{2\mathrm{i}\omega_0 T^n}\frac{1}{4\mathrm{i}T^n}\frac{\partial}{\partial\alpha}[\tau^n\,\mathrm{sinc}(2\alpha\tau^n T^n)] = \frac{1}{2\mathrm{i}}\sum_n \mathrm{e}^{2\mathrm{i}\omega_0 T^n}(\tau^n)^2\,\mathrm{sinc}'(2\alpha\tau^n T^n), \end{aligned}$$

so that $|W_{q1}| \sim \frac{N\tau^2}{2}$. The second term in (D.3) is estimated similarly to (A.16)–(A.18):

$$\begin{aligned} |W_{q2}| &= \left|\sum_n \mathrm{e}^{2\mathrm{i}\omega_0 T^n}T^n\int_{-\tau^n/2}^{\tau^n/2}\mathrm{e}^{4\mathrm{i}\alpha T^n u}\mathrm{d}u\right| = \left|\sum_n \mathrm{e}^{2\mathrm{i}\omega_0 T^n}T^n\tau^n\,\mathrm{sinc}(2\alpha\tau^n T^n)\right| \\ &\approx \tau^0\,\mathrm{sinc}(2\alpha\tau^0 T^0)\left|\sum_n T^n\mathrm{e}^{-2i\omega_0 T^n}\right| \lesssim \tau^0 N|\max(T^n)| \ll |W_{q1}|, \end{aligned}$$

and we see that it is negligible compared to the first term because $|T^n| \ll \tau$.

Thus, we will compare $W_q \approx W_{q1}$ against the expression (cf (A.6))

$$W_{q(RA)}(\boldsymbol{y},\boldsymbol{z}) \overset{\text{def}}{=} W_A(\boldsymbol{y},\boldsymbol{z})\cdot W_{qR}(\boldsymbol{y},\boldsymbol{z}),$$

where $W_A(\boldsymbol{y},\boldsymbol{z})$ is given by (15), and for the factor $W_{qR}(\boldsymbol{y},\boldsymbol{z})$ we have (cf (31), (32)):

$$W_{qR}(\boldsymbol{y},\boldsymbol{z}) = \int_\chi \overline{A(u_y^0)}u_z^0 A(u_z^0)\,\mathrm{d}t = \frac{(\tau^0)^2}{2\mathrm{i}}w_p'(2\alpha\tau^0 T^0) = \frac{(\tau^0)^2}{2\mathrm{i}}\,\mathrm{sinc}'(2\alpha\tau^0 T^0). \tag{D.4}$$

Similarly to (A.9), we write

$$2\mathrm{i}(W_q - W_{q(RA)}) = \sum_n \mathrm{e}^{2\mathrm{i}\omega_0 T^n}[(\tau^n)^2\,\mathrm{sinc}'(2\alpha\tau^n T^n) - (\tau^0)^2\,\mathrm{sinc}'(2\alpha\tau^0 T^0)].$$

Then, using the Taylor formula to approximate $\mathrm{sinc}'(2\alpha\tau^n T^n)$ (cf (A.14)):

$$\mathrm{sinc}'(2\alpha\tau^n T^n) \approx \mathrm{sinc}'(2\alpha\tau^0 T^0) - 2\alpha\tau^0 \mathcal{T}^n\,\mathrm{sinc}''(2\alpha\tau^0 T^0),$$

we obtain

$$\mathrm{i}(W_q - W_{q(RA)}) = \mathrm{e}^{\mathrm{i}\Phi_0}(-2\tau^0 S_q)\sum_n T^n\,\mathrm{e}^{-2\mathrm{i}\omega_0\mathcal{T}^n} = -2\tau^0 S_q\,\mathrm{e}^{\mathrm{i}\Phi_0}\frac{\mathrm{i}N}{2\omega_0}Y_1\,\mathrm{sinc}'\,Y_1,$$

where Y_1 is introduced right after equation (A.18), and

$$S_q = \mathrm{sinc}'(2\alpha\tau^0 T^0) + \alpha(\tau^0)^2\,\mathrm{sinc}''(2\alpha\tau^0 T^0).$$

The second term in the expression for S_q dominates because $\alpha\tau^2 \gg 1$. Then, the error due to the factorization of W_q can be estimated similarly to (A.19):

$$\frac{|\max(W_q - W_{q(RA)})|}{|\max W_{q(RA)}|} \sim \frac{2}{\omega_0\tau^0}Y_1 S_q \approx \frac{2}{\omega_0\tau^0}Y_1\frac{B}{2\tau}\tau^2 \sim \frac{B}{\omega_0}, \tag{D.5}$$

which is of the same order of magnitude as the error of the factorization of W, see (A.19). Hence, for the overall factorization error in (29) we have the same estimate: $\mathcal{O}\big(\frac{B}{\omega_0}\big)$.

References

[1] Tsynkov S V 2009 On SAR imaging through the Earth's ionosphere *SIAM J. Imaging Sci.* **2** 140–82
[2] Smith E M and Tsynkov S V 2011 Dual carrier probing for spaceborne SAR imaging *SIAM J. Imaging Sci.* **4** 501–42
[3] Gilman M, Smith E and Tsynkov S 2013 Reduction of ionospheric distortions for spaceborne SAR with the help of image registration *Inverse Problems* **29** 054005
[4] Ginzburg V L 1964 *The Propagation of Electromagnetic Waves in Plasmas (International Series of Monographs on Electromagnetic Waves* vol 7*)* (Oxford: Pergamon)
[5] Landau L D and Lifshitz E M 1984 *Electrodynamics of Continuous Media (Course of Theoretical Physics.* vol 8*)* (Oxford: Pergamon) (translated from the second Russian edition by J B Sykes, J S Bell and M J Kearsley, second Russian edition revised by Lifshits and L P Pitaevskii)
[6] Gail W B 1998 Effect of Faraday rotation on polarimetric SAR *IEEE Trans. Aerospace Electron. Syst.* **34** 301–8
[7] Wright P A, Quegan S, Wheadon N S and Hall C D 2003 Faraday rotation effects on L-band spaceborne SAR data *IEEE Trans. Geosci. Remote Sens.* **41** 2735–44
[8] Freeman A and Saatchi S S 2004 On the detection of Faraday rotation in linearly polarized L-band SAR backscatter signatures *IEEE Trans. Geosci. Remote Sens.* **42** 1607–16
[9] Meyer F J and Nicoll J B 2008 Prediction, detection, and correction of Faraday rotation in full-polarimetric L-band SAR data *IEEE Trans. Geosci. Remote Sens.* **46** 3076–86
[10] Jehle M, Rüegg M, Zuberbühler L, Small D and Meier E 2009 Measurement of ionospheric Faraday rotation in simulated and real spaceborne SAR data *IEEE Trans. Geosci. Remote Sens.* **47** 1512–23
[11] Lee J-S and Pottier E 2009 *Polarimetric Radar Imaging from Basics to Applications (Optical Science and Engineering)* (Boca Raton, FL: CRC Press)
[12] Parker S P (ed) 2002 *McGraw-Hill Dictionary of Scientific and Technical Terms* 6th edn (New York: McGraw-Hill)
[13] ITU Radio Regulations 2008 www.itu.int/pub/R-REG-RR-2008 (vol 1, article 2, p 27)
[14] Le Toan T *et al* 2011 The BIOMASS mission: mapping global forest biomass to better understand the terrestrial carbon cycle *Remote Sens. Environ.* **115** 2850–60
[15] Cheney M 2001 A mathematical tutorial on synthetic aperture radar *SIAM Rev.* **43** 301–12
[16] Cutrona L J 1990 Synthetic aperture radar *Radar Handbook* 2nd edn ed M Skolnik (New York: McGraw-Hill) chapter 21

[17] Cheney M and Borden B 2009 *Fundamentals of Radar Imaging (CBMS-NSF Regional Conference Series in Applied Mathematics* vol 79*)* (Philadelphia, PA: SIAM)
[18] Cumming I G and Wong F H 2005 *Digital Processing of Synthetic Aperture Radar Data. Algorithms and Implementation* (Boston, MA: Artech House Publishers)
[19] Born M and Wolf E 1999 *Principles of Optics: Electromagnetic Theory of Propagation, Interference and Diffraction of Light* (with contributions by A B Bhatia, P C Clemmow, D Gabor, A R Stokes, A M Taylor, P A Wayman and W L Wilcock) 7th edn (Cambridge: Cambridge University Press)
[20] Jakowatz C V Jr, Wahl D E, Eichel P H, Ghiglia D C and Thompson P A 1996 *Spotlight-Mode Synthetic Aperture Radar: A Signal Processing Approach* (New York: Springer)
[21] Davies K and Smith E K 2002 Ionospheric effects on satellite land mobile systems *IEEE Antennas Propag. Mag.* **44** 24–31
[22] Meyer F J 2011 Performance requirements for ionospheric correction of low-frequency SAR data *IEEE Trans. Geosci. Remote Sens.* **49** 3694–702
[23] Gilman M, Smith E and Tsynkov S 2012 A linearized inverse scattering problem for the polarized waves and anisotropic targets *Inverse Problems* **28** 085009
[24] Goodman J W 1976 Some fundamental properties of speckle *J. Opt. Soc. Am.* **66** 1145–50
[25] Oliver C J 1986 The interpretation and simulation of clutter textures in coherent images *Inverse Problems* **2** 481
[26] Quegan S 1990 Interpolation and sampling in SAR images *IEEE Trans. Geosci. Remote Sens.* **28** 641–6
[27] Lopès A, Garello R and Le Hégarat-Mascle S 2008 Speckle models *Processing of Synthetic Aperture Radar Images (Digital Signal and Image Processing Series)* ed H Maître (New York: Wiley) pp 87–142
[28] Oliver C and Quegan S 1998 *Understanding Synthetic Aperture Radar Images* (Boston, MA: Artech House Publishers)
[29] Massonnet D and Souyris J-C 2008 *Imaging with Synthetic Aperture Radar (Engineering Sciences: Electrical Engineering)* (Lausanne: CRC Press)
[30] Ryaben'kii V S and Tsynkov S V 2007 *A Theoretical Introduction to Numerical Analysis* (Boca Raton, FL: Chapman and Hall)
[31] Chorin A J and Hald O H 2006 *Stochastic Tools in Mathematics and Science (Surveys and Tutorials in the Applied Mathematical Sciences* vol 1*)* (New York: Springer)
[32] Roberts P H 2007 Alfvén's theorem and the frozen flux approximation *Encyclopedia of Geomagnetism and Paleomagnetism* ed D Gubbins and E Herrero-Bervera (Dordrecht: Springer) pp 7–11
[33] Garnier J and Sølna K 2013 A multiscale approach to synthetic aperture radar in dispersive random media *Inverse Problems* **29** 054006
[34] Oraevsky V N 1984 Kinetic theory of waves *Basic Plasma Physics: Selected Chapters, Handbook of Plasma Physics* vol 1 ed A A Galeev and R N Sudan (Amsterdam: North-Holland) pp 243–78